filter set (ex/em 615-665/695-770). Tissues were then excised from the mice and fluorescent images of the tissues were obtained. Imaging parameters were selected and implemented using the instrument, Living Image 2.5 software. Bright field photographs were obtained for each imaging time. The merged bright field photographs and fluorescent images were generated using Living Image 2.5 software.

### 2.13. Transmission electron microscopy (TEM) analysis of liver

BALB/c mice were treated with 0.6 mg/mouse (about 30 mg/kg, 70 nm) or 2 mg/mouse (about 100 mg/kg, 300 and 1000 nm) silica particles of each particle size and PBS (control) by intravenous injection. After 24 h, the tissues and organs such as brain, heart, lung, liver, kidney, spleen and lymph node, were excised and fixed in 2.5% glutaraldehyde for 2 h. Small pieces of tissue sample were then washed with phosphate buffer three times and postfixed in sodium cacodylate-buffered 1.5% osmium tetroxide for 60 min at 4 °C, block stained in 0.5% uranyl acetate, dehydrated through a series of ethanol concentrations, and embedded in Epon resin (TAAB). Ultrathin sections were stained with uranyl acetate and lead citrate. The samples were examined under a Hitachi electron microscope (H-7650).

### 2.14. Living cell counting and DNA damage determination in isolated primary hepatocytes from silica particle-treated mice

Female BALB/c mice were treated with 2 mg/mouse (about 100 mg/kg) silica particles of each particle size (70, 100, 300 and 1000 nm) and PBS (control) by intravenous injection. After 5 h, parenchymal hepatocytes were isolated according to the *in situ* two-step collagenase perfusion technique. Briefly, the liver was perfused with 25 ml of 10 mM Hepes buffered calcium- and magnesium-free Hanks' balanced salt solution (HBSS) containing 190 mg/l EGTA (DOJINDO) for 5 min. The liver was then perfused with 40 ml of HBSS containing 250 mg/l trypsin inhibitor, 500 mg/l collagenase and 550 mg/l $CaCl_2$ for 10 min. The liver was then excised and the cells dispersed in HBSS. The cells were then centrifuged at 50 × g at 4 °C for 1 min. The resulting pellet was resuspended in 20 ml of L15 medium containing 5% FCS, 1 μM dexamethasone and 1 μM insulin and centrifuged at 50 × g at 4 °C for 1 min. This step was repeated 3 times. The resulting pellet was resuspended in medium and living cells were counted using trypan blue staining. Endogenous DNA damage in isolated primary parenchymal hepatocytes from mice treated with nSP70, nSP300, mSP1000 and PBS (control) was analyzed by alkaline comet assay as described above.

### 2.15. Statistical analysis

Statistical comparisons between groups were performed by one-way ANOVA with Bonferroni test as a *post hoc* test. The level of significance was set at $P < 0.05$.

## 3. Results and discussion

### 3.1. Physicochemical properties of various sized silica particles and QD

The first step for ensuring the biosafety of NMs are to evaluate whether the NMs could penetrate the epithelial barriers, could eventually become absorbed systemically, and more importantly, whether they could be responsible for acute/chronic side effects. In this context, here, we evaluated whether the nSP and QD could penetrate into the skin of BALB/c mice following dermal exposure. Prior to undertaking the skin penetration study, we first analyzed the physicochemical properties of the commercially available silica particles of 70, 300 and 1000 nm in diameter (nSP70, nSP300 and mSP1000, respectively). Close examination of the silica particles of different particle sizes by TEM revealed that all silica particles used in this study were smooth-surfaced spherical particles and in size category the primary particle sizes were approximately uniform (Fig. 1a–f). According to technical datasheet, surface textures of all silica particles were plain and nonporous. The specific surface area was calculated by means of the following equation; $s = 6/d\rho$ (where s, specific surface area ($m^2/g$); ρ, density (g/cc); d, diameter (μm)). The specific surface area of nSP70, nSP300 and mSP1000 calculated using this equation was 43, 10 and 3 $m^2/g$, respectively. In addition, all silica particles used in this study was not modified with any functional groups. These physicochemical properties were summarized in Table 1. From the results of mean particle size in solution, it was suggested that the silica particles used in this study remained as stable well-dispersed particles in solution, and not as aggregates. Thus, these particles are ideally suited as optimal sample to evaluate if and whether their biodistribution and biological effect depend on the particle size. As well as silica particles, the shape, size distribution and zeta potential of QD were evaluated. Surface of QD used in this study were coated with polyethylene glycol (PEG). QD were enhanced using silver for TEM analysis, because silver selectively deposits on the QD [27]. From the results of TEM analysis, QD were also spherical particles, and in terms of size category the primary particle sizes (about 35 nm) were approximately uniform. The size distribution spectrum of QD in a neutral solvent showed two peaks, and the average particle size of peaks 1 and 2 was about 35 and 300 nm, respectively.

### 3.2. Analysis of transdermal penetration and biodistribution of nanosilica and QD applied on the skin

We next used TEM to determine whether nSP with a particle size below 100 nm would penetrate the skin after topical application. As a result, the 28-day application of nSP70 to mice showed that nSP70 entered not only the skin (Fig. 2a), the regional lymph nodes (Fig. 2b) and the parenchymal hepatocytes present in liver (Fig. 2c, d) but also the cerebral cortex (Fig. 2e) and the hippocampus (Fig. 2f). Surprisingly, penetration of nSP70 into the liver was also detected, and some of the nSP70 that entered the parenchymal hepatocytes were found to be distributed throughout the cytoplasm and inside the nucleus (Fig. 2c) and mitochondria (Fig. 2d). Localization of nSP70 in the nucleus was also detected in the skin and the lymph node (Fig. 2a, b). Next, the skin permeability of QD was evaluated. We found that QD penetrated the stratum corneum and entered the skin (Fig. 2g), lymph node (Fig. 2h), liver (Fig. 2i, j), cerebral cortex (Fig. 2k) and hippocampus (Fig. 2l). In addition, some of the QD that entered the skin (Fig. 2g), lymph node (Fig. 2h) and parenchymal hepatocytes (Fig. 2i) were detected inside the nucleus, similar to nSP70. We considered that the well-dispersed portion of QD showed skin permeability. It has been reported that QD can enter the skin by transdermal exposure under ultraviolet radiation [27]. However, for the first time we have revealed that nSP and QD penetrate the skin and enter tissues such as the lymph node, liver and brain under normal conditions.

### 3.3. Analysis of biological effects induced by nanosilica and QD

The next step for the biosafety should include analyzing their biological effects against skin, brain, liver and lymph node. Consequently, first, in order to assess the biological response in the skin as a part of 28-day application of nSP70, we tried to detect the apoptotic cells by using Terminal Deoxynucleotidyl Transferase-Mediated X-dUTP Nick-End Labeling (TUNEL) staining. As a result, while a few TUNEL-positive cells were detected in water-applied mice skin (control) (Fig. 3a), a number of TUNEL-positive cells (expressed in red) were detected in nSP70-applied mice skin (Fig. 3b). The ratio of TUNEL-positive cells in the skin sections of mice transdermally-applied with nSP70 tended to increase compared to mice transdermally-applied with water (control). In one of two nSP70-applied mice, the ratio of TUNEL-positive cells in the skin section was dominantly increased (Fig. 3c). This result suggested that the transdermal application of nSP70 induced the cellular damage in the skin. On the basis of this result and transdermal absorption test results, we are now evaluating higher cerebral function, hepatic drug metabolism, and the immune system of mice after topical nSP exposure. Moreover, it is necessary to evaluate the influence of well-dispersed NMs on nuclear and mitochondrial functions, because we found that nSP70 and QD enter into these specific organelles. These results also suggest that systemic safety analysis (hazard analysis) of an NM is highly important for ensuring its safety. Because nSP70 and QD can

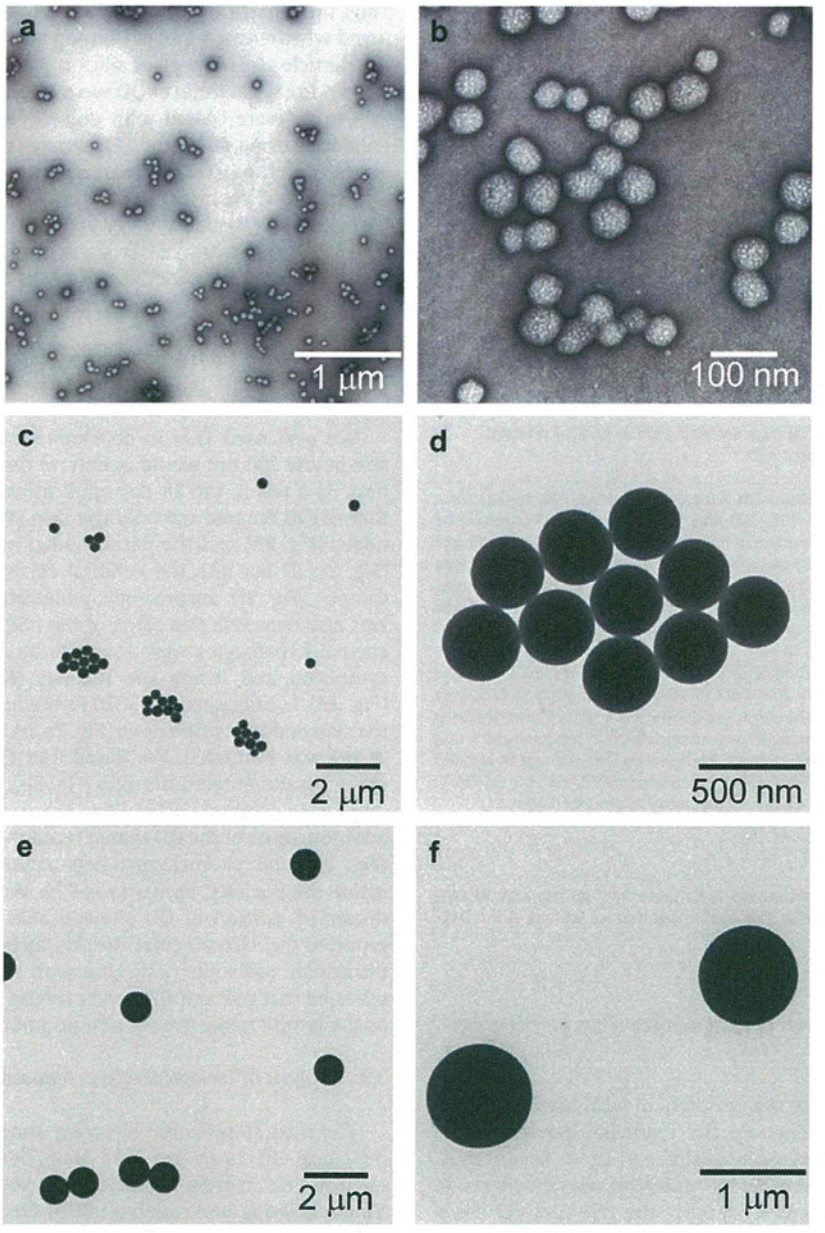


**Fig. 1.** Transmission electron microscopy (TEM) analysis of silica particles. a–f, TEM photomicrographs of silica particles used in this study: nSP70 (a and b), nSP300 (c and d) and mSP1000 (e and f). Each type of sized silica particles existed as scattered and spheroidal. Scale bars: 1 μm (a and f), 100 nm (b), 500 nm (d) and 2 μm (c and e).

penetrate the skin barrier, which is the most rigid biological barrier, we believe that analysis of oral and pulmonary exposure should also be included in ensuring the biosafety of NMs.

Collectively, these observations clearly show that nSPs and QD of less than 100 nm in diameter invade the body through the skin, suggesting that human beings are at high risk of exposure to NMs through the blood stream. Consequently, we analyzed the distribution and biological effects of NMs with a focus on the region level and the systemic level. Because nSPs have already been put into practical use in cosmetics, firstly, we evaluated the intracellular

**Table 1**
Summary of the physicochemical properties of silica particles.

| | Primary particle size (nm)[a] | Hydrodynamic diameter (nm) | Mean zeta potential (mV) | pH | Surface texture[a] | Porosity[a] | Surface area ($m^2/g$)[b] | Functional group[a] |
|---|---|---|---|---|---|---|---|---|
| nSP70 | 70 | 77.0 ± 0.4 | −21.6 ± 4.5 | 7.4 | Plain | Nonporous | 43 | None |
| nSP300 | 300 | 269.3 ± 2.1 | −31.3 ± 6.5 | 7.5 | Plain | Nonporous | 10 | None |
| mSP1000 | 1000 | 1187 ± 25.2 | −37.7 ± 4.6 | 7.9 | Plain | Nonporous | 3 | None |

Mean particle size and zeta potential in solution of silica particles are expressed as mean ± S.D. ($n = 3$).

[a] Information from technical datasheet of products.

[b] The specific surface area was calculated by means of the following equation; $s = 6/d\rho$ (where s, specific surface area ($m^2/g$); $\rho$, density (g/cc); $d$, diameter (μm)).

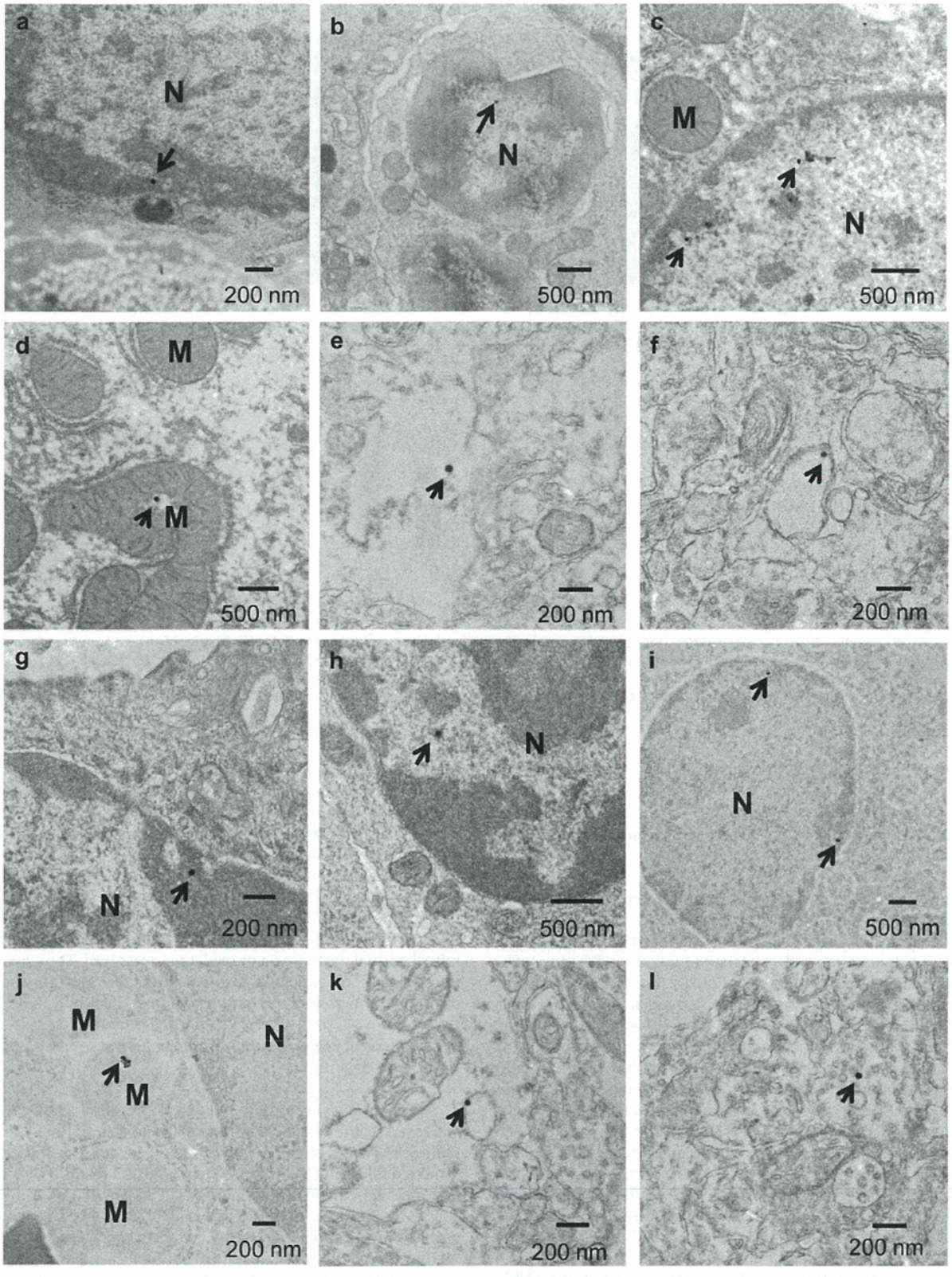


**Fig. 2.** TEM analysis of skin, lymph node, liver and brain samples from mice after 28-days of dermal exposure to silica nanoparticles and quantum dots. a–c, nSP70 (arrows) were present in the nucleus of skin (a), cervical lymph node (b), and parenchymal hepatocytes (c). d, nSP70 were also detected in the mitochondria of parenchymal hepatocytes. e–f, nSP70 were found in neuron of the cerebral cortex (e) and the hippocampus (f). g–h, QD (arrows) were present in the nucleus of skin (g), cervical lymph node (h) and parenchymal hepatocytes (i), similar to nSP70. j, In parenchymal hepatocytes, QD were detected in the mitochondria (j). k–l, QD were found in neuron of the cerebral cortex (k) and the hippocampus (l). N: nucleus; M: mitochondria. Scale bars: 200 nm (a, e–g, and j–l), 500 nm (b–d, h and i).

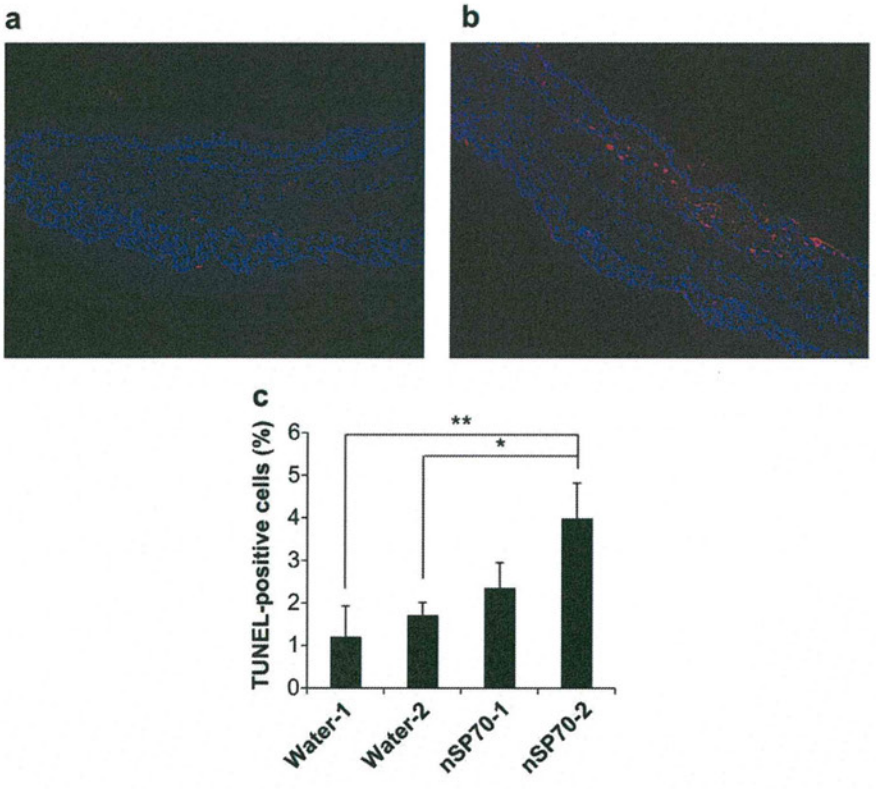


**Fig. 3.** Detection of apoptotic cells in silica nanoparticles-applied mice skin. a, b, Representative images from TUNEL stained skin section in water- (control, a) and nSP70- (b) applied mice were shown. Nuclei and TUNEL-positive cells were represented in blue and red, respectively. Original magnification, ×200. c, For quantification of TUNEL-positive cells, approximately 1000 cells were randomly selected from 3 different areas in each section and two animals and counted the numbers of positive cells expressed as a percentage of the total (c). Data shown are average means (±SD) of each treated group. * Significant increase ($P < 0.005$) compared with Water-2. ** Significant increase ($P < 0.001$) compared with Water-1.

distributions and biological responses of NM size in skin with a focus on nSP.

### 3.4. Analysis of intracellular distribution of silica particles in human keratinocyte

Presently, many modern cosmetic or sunscreen products contain nano-sized components, such as titanium dioxide ($TiO_2$), zinc oxide (ZnO) and amorphous silica particles. Nano-sized $TiO_2$ and ZnO are colorless substances and reflect/scatter ultraviolet (UV) more efficiently than their larger counterparts [28,29]. Amorphous nanosilica particles (nSPs) are used in large quantities and are one of the most important ingredients in the cosmetic industry, especially for their light-diffusing and absorption properties. Extensive consumption of these NM-supplemented cosmetic and food products has naturally raised the question as to whether these NMs could penetrate the skin, would eventually become absorbed systemically, and more importantly, whether they could be responsible for acute/chronic side effects. In the present study, we revealed that well-dispersed nSP could penetrate into and pass through the skin. Interestingly, we found that nSP70 migrated into the blood stream and passed into tissues such as liver. Moreover, nSP70 invaded specific organelles such as the nucleus and mitochondria. In view of these observations, we next examined the relation between the intracellular distribution and biological effects of nSP, which are the most important NMs in our daily life.

To determine the intercellular location of silica particles, we used TEM to examine the HaCaT cells that were treated with 100 μg/ml of nSP70, nSP300, or mSP1000. TEM examination revealed the presence of mSP1000 and nSP300 only in the endosome (Fig. 4a, b, arrows). mSP1000-treated cells were also found to contain a large number of lysosomes (Fig. 4a). In contrast, only in the nSP70-treated cells nSP70s were present in the cytoplasm as well as in the nucleus (Fig. 4c, d, arrow heads). Furthermore, nSP70s were accumulated in the nucleolus (Fig. 4e, f, arrows). Recently, it has been reported that the intercellular localization of NM is possibly linked to the induction of harmful effects. For example, the localization of silver nanoparticles in the nucleus and mitochondria may be related to mitochondrial dysfunction or oxidative stress [30]. Thus, analysis of intracellular localization enables us to provide important and useful information to predict the hazard to human health.

### 3.5. Analysis of cell-growth inhibition and genotoxicity induced by silica particles

Next, we investigated the biological effects of nSP. To this end, we assessed the effects of various particle size nSP on the proliferation of HaCaT cells. As shown in Fig. 5a, cell proliferation was inhibited following treatment with nSP70 and nSP300 in both dose and size dependent manner. The half maximal (50%) inhibitory concentration ($IC_{50}$) of nSP70 and nSP300 for inhibiting cell proliferation was 323 and 3966 μg/ml, respectively. We were, however, unable to calculate the $IC_{50}$ of nSP1000. Taken together, these results suggested that smaller sized silica particles inhibited the growth of HaCaT cells more strongly than the larger particles. In addition, we assessed the effects of QD on the proliferation of HaCaT cells. As the result, we indicated that the effect to cell proliferation of QD was predominantly lower than nSP70 at same

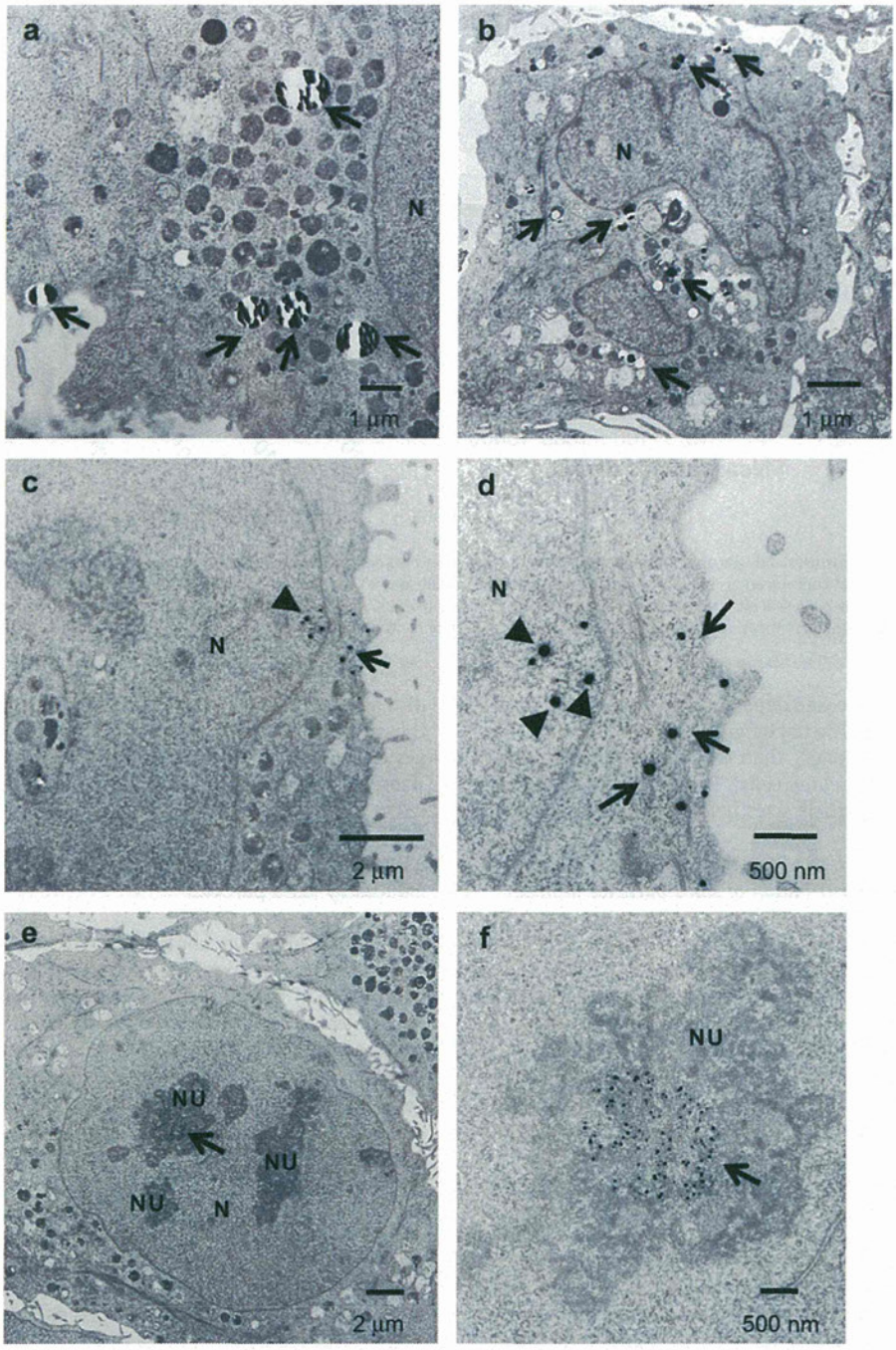


**Fig. 4.** TEM analysis of HaCaT cells treated with silica particles. a–e, Silica particles (arrows) were found in HaCaT cells treated for 24 h with 100 μg/ml of mSP1000 (a), nSP300 (b), and nSP70 (c, d, and e). In panels c and d, arrow heads show the presence of nSP70 in the nucleus, and in panels e and f, arrows show the presence of nSP70 in the nucleolus. Panels d and f are same as panels c and e at higher magnifications, respectively. N: nucleus; NU: nucleolus. Scale bars: 1 μm (a and b), 2 μm (c and e) and 500 nm (d and f).

concentrations (particles/ml) (Fig. 5b). This result suggested that the biological effects of NMs were different by material.

On the basis of the nuclear entry of nSP70 *in vivo* and *in vitro*, we next evaluated the mutagenicity of silica particles using *S. typhimurium* strains TA98 and TA100 (Ames test). None of the nSP that we tested induced mutation in TA98 strain when used at the indicated concentrations (Fig. 6a). By contrast, nSP of all sizes induced mutagenicity in TA100 strain at the highest dose of treatment (810 μg/ml) (Fig. 6b). At lower doses (30 and 90 μg/ml) of treatment, only nSP70 induced mutation in TA100 strain (Fig. 6b). Thus, the results obtained from the Ames test suggest that the mutagenicity of the silica particles increased with the decreasing particle size. Next, we used the comet assay to analyze DNA single strand breaks in nSP-treated HaCaT cells. In cells treated with PBS (negative control) for 3 h, the average tail length was 23.3 μm (Fig. 6c). In cells treated with 90 μg/ml of nSP70, nSP100, nSP300, or mSP1000, the average tail lengths were 102.9 μm (Fig. 6d), 88.8 μm (data not shown), 30.5 μm (Fig. 6e), and 22.5 μm (Fig. 6f), respectively.

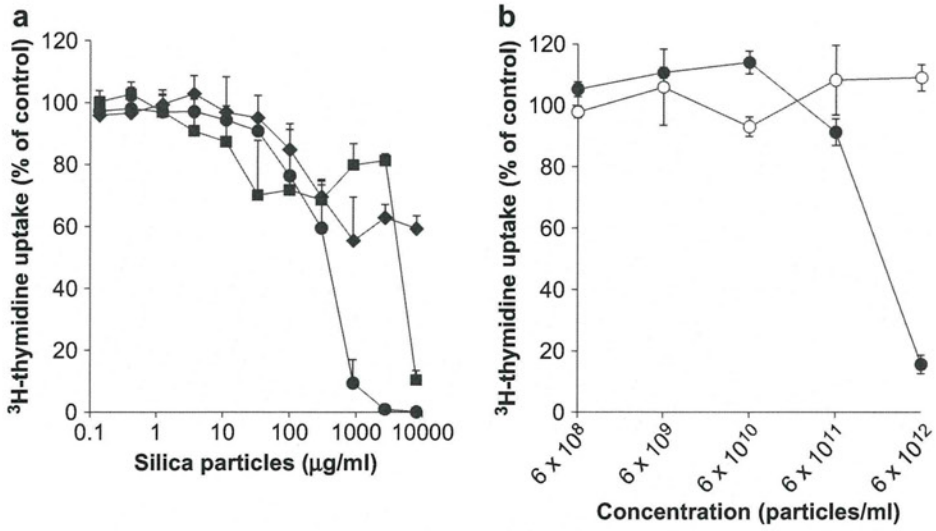


**Fig. 5.** Effect of various sized silica particles and QDs on cell proliferation. a) In order to assess the biological effects according to particle size, proliferation of HaCaT cells following 24 h of incubation with the indicated concentrations of nSP70 (closed circle), nSP300 (closed square) and mSP1000 (closed diamond) were measured using the tritium thymidine uptake assay. b) In order to assess the biological effects according to the material, proliferation of HaCaT cells following 24 h of incubation with the indicated concentrations of nSP70 (closed circle) and QD (opened circle) were measured. Results shown as relative rates (% of control). Each data point represents mean ± SD ($n = 3$).

The average tail lengths increased depending on the dose and size of the silica particles (Fig. 6g). The tail lengths found in the nSP70- and nSP100-treated cells were longer than those found in the positive control cells (0.2 mM $H_2O_2$ treated cells). These findings suggest the possibility that nSP with particle sizes below 100 nm could induce mutation.

### 3.6. Analysis of in vivo biodistribution of silica particles in mice

We next analyzed biodistribution and biological effects in systemic level using silica particles-injected mice, because it was suggested that nSP moved to the blood stream from skin as described above. To elucidate the *in vivo* distribution of silica particles, we determined the distribution of silica particles following intravenous injection, by optical imaging analysis (Fig. 7a–c). Intense fluorescence was observed near the liver in all silica particle-treated mice immediately after treatment and this signal migrated to near the intestinal tract with time. Imaging of dissected liver from nSP300- or mSP1000-treated mice revealed that intense fluorescence was observed only around the gall bladder. In contrast, nSP70-derived fluorescence was observed throughout dissected liver. In addition, our preliminary results revealed that all silica particle-derived fluorescence was also observed in intestinal tract and feces (data not shown), suggesting that silica particles might be excreted in the bile after circulating systemically, in a manner independent of particle size.

To clarify detailed localization of silica particles in liver of nSP-injected mice, next we perform transmission electron microscopy (TEM) analysis (Fig. 7d–g). While silica particles of all sizes were found to be ingested into Kupffer cells, nSP70 and nSP300 were also observed in parenchymal hepatocytes. In the nSP70-treated group, particles were shown to be localized in the cytoplasm and nucleus of various tissues such as lung, kidney, spleen and lymph node (data not shown). Microscopic findings showed that with reduction in particle size, silica particle uptake into Kupffer cells tended to be decreased and in contrast, particle uptake into the cytoplasm of parenchymal hepatocytes tended to be increased (Fig. 7h). Surprisingly, sub-nuclear localization of particles was observed in nSP70-treated groups (Fig. 7e). These results confirmed that the distribution of nSPs with particle size less than 100 nm differ from those of submicron-sized silica particles. These data strongly suggested that we must distinguish nSPs from existing submicron-sized silica particles, and address specialized risk assessment for nSPs.

### 3.7. Analysis of cytotoxicity and genotoxicity in primary hepatocyte induced by silica particles

Subsequently, we confirmed whether the biological effects induced by nSP in liver in which silica particles accumulated. The liver is one of the most important tissue in the body, because the liver takes an important role in metabolism, discharge, detoxification, maintenance of homeostasis of the body fluid. Especially, hepatocyte plays a vital role as functions of the liver. Using primary hepatocyte isolated from silica particles-injected mice intravenously, cytotoxicity and DNA damage of hepatocyte were analyzed. As the result, cytotoxicity of hepatocyte from nSP300 and mSP1000-injected mice little occurred. On the other hand, hepatocyte from nSP70-injected mice indicated higher cytotoxicity than nSP300 and mSP1000-injected mice (Fig. 8a). Furthermore, DNA damage of hepatocyte was detected only in nSP70-injected mice as well as in HaCaT cells (Fig. 8b). These results also indicate that differences in biological effects such as cytotoxicity and genotoxicity are caused by differences in biodistribution of silica particles. And it suggests that accumulation of nSP into the liver and/or nucleus may lead to genotoxicity.

Thus, we also highly recommend including carcinogenicity test and reproductive and developmental toxicity test for ensuring biosafety of NMs. Additionally, because nSP70 were accumulated in the nucleus, we suggest evaluating the effect of an NM on protein synthesis to further ensure its biosafety.

Nuclear pores are made of large protein complexes that cross the nuclear envelope, the membrane bilayer that surrounds the nucleus of the eukaryotic cell, and the pores are about 30 nm in diameter [31,32]. Thus, it is unlikely that the nSP70, which has a mean diameter of about 70 nm, entered the nucleus through the nuclear pore. We hypothesize that the nSP70 might interact with the nuclear transporting proteins via specific- or non-specific

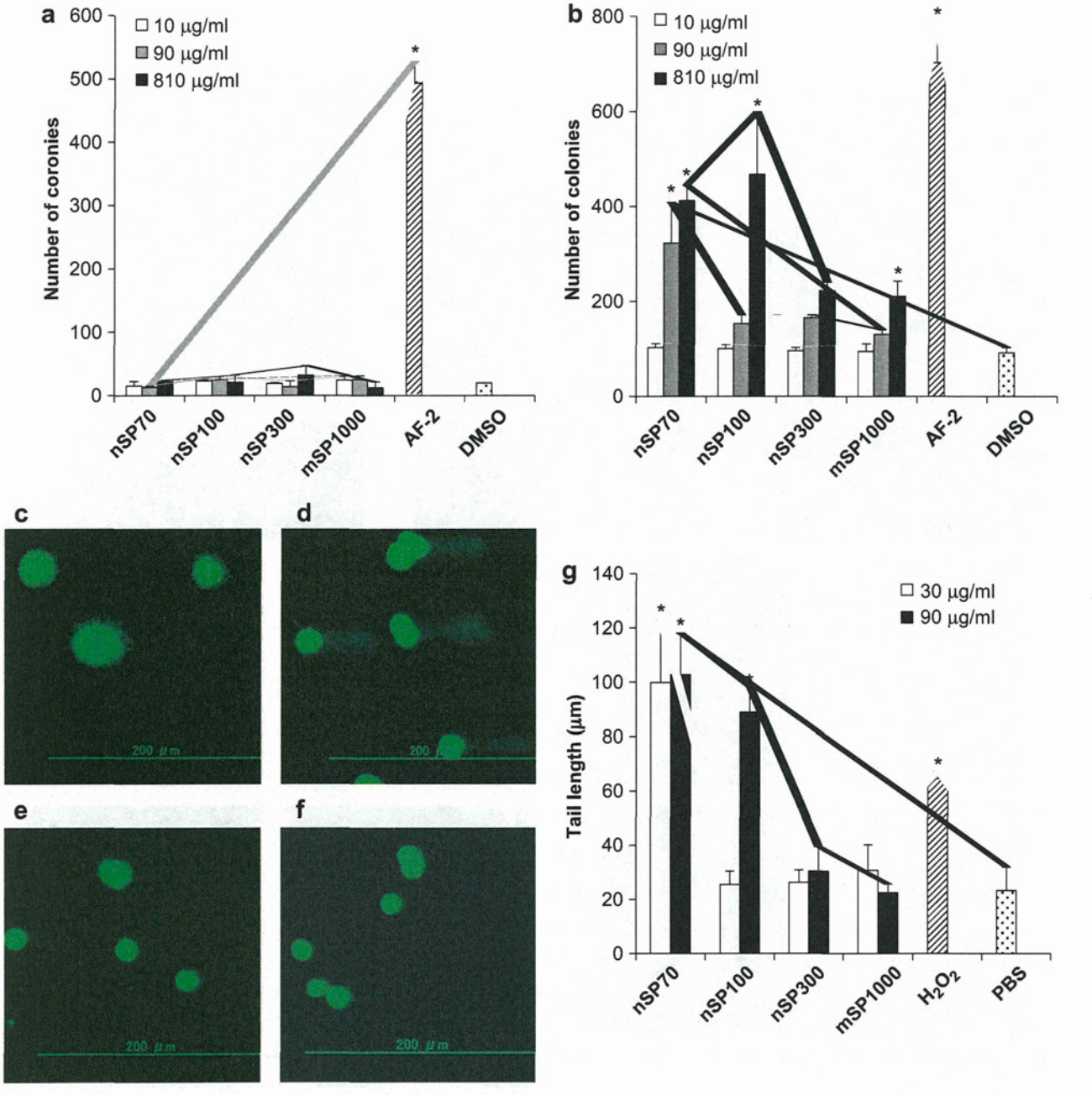


**Fig. 6.** Genotoxic effects of silica particles. a–b, Mutagenic effects of silica particles as determined by the Ames test. Dose-response of mutagenic effects of nSP70, nSP300, and mSP1000 on *S. typhimurium* strains: strain TA98 (a) and strain TA100 (b). The Ames test was performed as described in Methods. Values shown are mean ± SD ($n = 3$). *More than 2-fold increase compared to the medium-treated control (DMSO). AF-2, positive control. e–g, Detection of DNA strand breaks by the comet assay. Representative fluorescence images of HaCaT cells treated for 3 h with PBS (negative control) (c), or 90 μg/ml of nSP70 (d), nSP300 (e), and mSP1000 (f). Scale bar: 200 μm e, Column graph showing the tail lengths after being incubated with 30 μg/ml (open column) and 90 μg/ml (closed column), respectively, of nSP70, nSP300, and mSP1000, and 0.2 mM $H_2O_2$ (positive control) for 3 h. Data shown are average means (±SD) of at least 16 cells for each sample. Results shown are representative of more than three independent experiments. *Significant increase ($P < 0.01$) compared with the negative control, PBS.

interactions, and the nSP70/protein complexes are then transported into the nucleus. To test this hypothesis, we are currently pursuing a proteome-based approach to identify nSP70-interacting proteins.

Recently, commercially available amorphous silica-based products were subjected to various toxicological tests including acute and repeated dose toxicity, genotoxicity, carcinogenicity and reproductive toxicity [33]. According to this report, amorphous silica particles are non-toxic. Although the primary particle sizes of the amorphous silica used in these toxicological studies were between 1 and 100 nm, the ECETOC 2006 report stated that they did not exist as primary particles, but existed only as aggregates of particle sizes between 100 nm and 1 μm. The ECETOC 2006 report, however, did not exclude the possibility that materials having particle sizes below 100 nm might be developed and available for use in the future. In contrast to the results described in the ECETOC report, results of our present

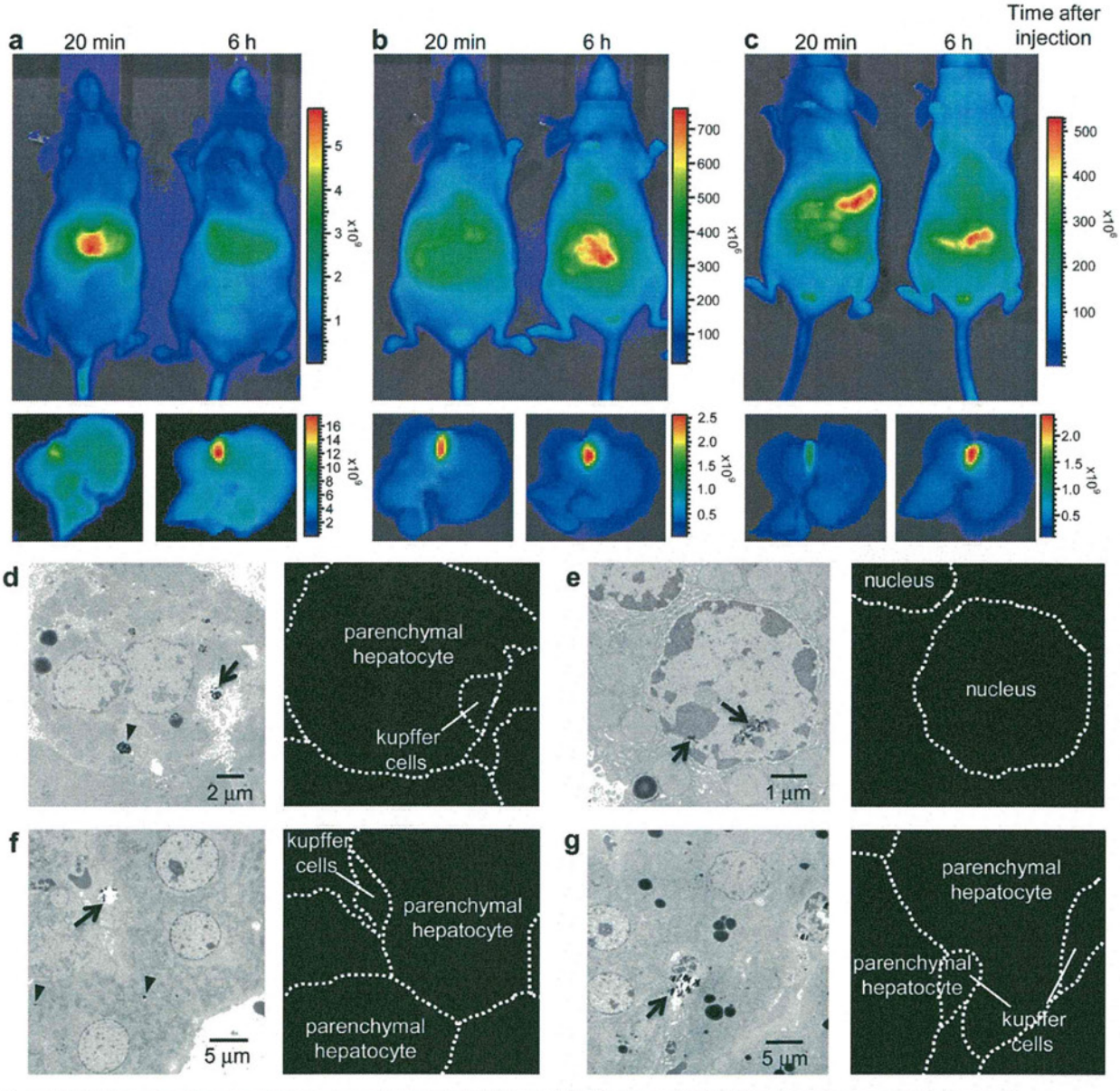


h

| | nSP70 | nSP300 | mSP1000 |
|---|---|---|---|
| Englobement in Kupffer cell | ++ | ++ | +++ |
| Localization in cytoplasm of hepatocyte | +++ | + | - |
| Localization in nucleus of hepatocyte | + | - | - |

**Fig. 7.** Biodistribution analysis of silica particles at macro- and micro levels. A–C, Macro level analysis: optical imaging of fluorescently labeled silica particles in live mice and excised liver. DY676-labeled silica particles (a, nSP70, b, nSP300 and c, mSP1000, 100 mg/kg) were intravenously injected into female hairless mice. Twenty min and 6 h after injection, optical images were acquired using a Xenogen IVIS 200 imaging system. The signal intensity in the region of interest is expressed as photons (p) per second (sec) per centimeter squared ($cm^2$) per steradian (sr) (a steradian is a unit of solid angle). d–f, Micro level analysis: BALB/c mouse liver injected with 30 mg/kg (nSP70) or 100 mg/kg (nSP300 and mSP1000) nSPs was observed by TEM. d, arrow, nSP70, f arrow, nSP300, g, mSP1000 were phagocytosed in Kupffer cells. d, arrow head, nSP70 and f, arrow head, nSP300 were also detected in cytoplasm of parenchymal hepatocytes. Interestingly, e, nSP70 entered the nucleus of the parenchymal hepatocytes. Arrows and arrow heads indicate silica particles. Scale bar, d, 2 μm, e, 1 μm and f, g, 5 μm. H, Localization of each silica particle in liver is summarized. Amount of silica particles were shown as follows; –: Not detected, +: small, ++: middle, +++: large.

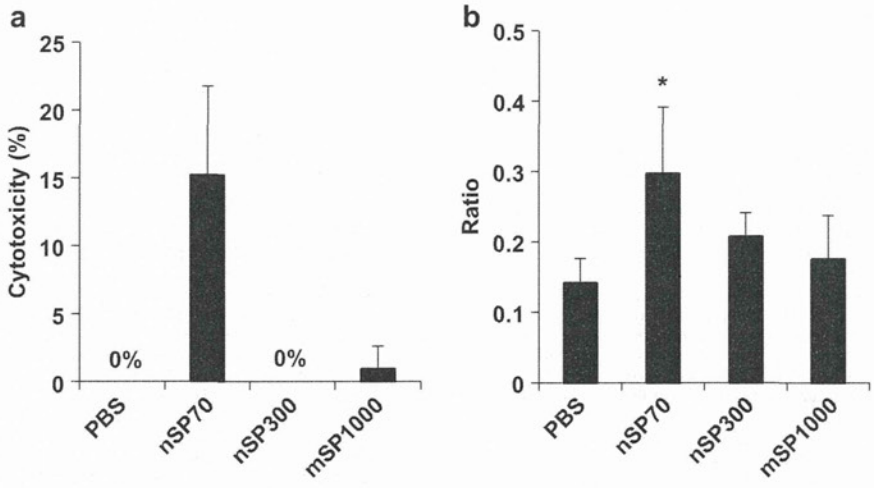


**Fig. 8.** Liver toxicity analysis in parenchymal hepatocytes. a, Cytotoxicity of parenchymal hepatocytes isolated from nSP-injected mice 5 h after injection by trypan blue stain. b, Detection of DNA strand breaks ratio of parenchymal hepatocytes isolated from nSP-injected mice 5 h after injection. Data are shown as mean ± SD; comet tails from at least 16 cells were counted in each sample. All data are representative of more than three slides. * Represents significant difference from the control group ($P < 0.01$).

study showed that well-dispersed nSP70 could indeed penetrate the skin barrier and cause systemic exposure, thus suggesting that the well-dispersed NMs have to be viewed as new entities and tested accordingly for ensuring their biosafety. It is known that the asbestos-related health hazard, symptoms of mesothelioma, appears after prolonged exposure to asbestos particles (average of 40 years, shortest around 20 years) [34–37]. Because of this and also in view of the growing demand for the NMs in various fields, there is a clear and urgent need for in depth risk assessment of all NMs for safety use. Keeping in line with this idea and because it is not known whether exposure to NMs might cause initiation and/or progression of various diseases (e.g., atopic dermatitis, infectious disease, etc.), we have initiated more detailed and extensive safety analysis studies including relationships between the physicochemical properties (i.e., size, shape, and surface property) of an NM and its biodistribution, and analysis of the interaction of the NMs with allergens, gastrointestinal flora, and resident floras as contributing factors to human health in order to further ensure its biosafety.

## 4. Conclusions

This study revealed that, as compared with the bulk material of particle sizes above nanoscale (above 100 nm), well-dispersed amorphous nanosilica with a particle size of 70 nm shows different bio-properties with respect to skin penetration and nuclear entry. These bio-properties of nanosilica show the potential as a new functional material, but, reflecting these differences, nSP70 exert various adverse biological effects in regional and systemic level, such as DNA fragmentation. We consider that more information which provided by further studies of relation between physicochemical properties and biological responses, would lead to realization of an affluent society by the use of safe and useful NMs.

## Acknowledgments

This study was supported in part by Grants-in-Aid for Scientific Research from the Ministry of Education, Culture, Sports, Science and Technology of Japan, and from the Japan Society for the Promotion of Science (JSPS). This study was also supported in part by Health Labour Sciences Research Grants from the Ministry of Health, Labor and Welfare of Japan; by a Global Environment Research Fund from Ministry of the Environment; and by the Knowledge Cluster Initiative; and by The Nagai Foundation Tokyo; and by The Cosmetology Research Foundation; and by The Smoking Research Foundation.

## References

[1] Salata O. Applications of nanoparticles in biology and medicine. J Nanobiotechnology 2004;2(1):3.
[2] Aiso S, Yamazaki K, Umeda Y, Asakura M, Takaya M, Toya T, et al. Pulmonary toxicity of intratracheally instilled multiwall carbon nanotubes in male Fischer 344 rats. Ind Health; 2010 [Epub ahead of print].
[3] Chen J, Dong X, Zhao J, Tang G. *In vivo* acute toxicity of titanium dioxide nanoparticles to mice after intraperitioneal injection. J Appl Toxicol 2009;29(4):330–7.
[4] Geys J, Nemmar A, Verbeken E, Smolders E, Ratoi M, Hoylaerts MF, et al. Acute toxicity and prothrombotic effects of quantum dots: impact of surface charge. Environ Health Perspect 2008;116(12):1607–13.
[5] Heng BC, Zhao X, Xiong S, Ng KW, Boey FY, Loo JS. Toxicity of zinc oxide (ZnO) nanoparticles on human bronchial epithelial cells (BEAS-2B) is accentuated by oxidative stress. Food Chem Toxicol 2010;48(6):1762–6.
[6] Kocbek P, Teskac K, Kreft ME, Kristl J. Toxicological aspects of long-term treatment of keratinocytes with ZnO and TiO(2) nanoparticles. Small 2010; 6(17):1908–17.
[7] Liu S, Xu L, Zhang T, Ren G, Yang Z. Oxidative stress and apoptosis induced by nanosized titanium dioxide in PC12 cells. Toxicology 2010;267(1–3):172–7.
[8] Moos PJ, Chung K, Woessner D, Honeggar M, Cutler NS, Veranth JM. ZnO particulate matter requires cell contact for toxicity in human colon cancer cells. Chem Res Toxicol 2010;23(4):733–9.
[9] Murray AR, Kisin E, Leonard SS, Young SH, Kommineni C, Kagan VE, et al. Oxidative stress and inflammatory response in dermal toxicity of single-walled carbon nanotubes. Toxicology 2009;257(3):161–71.
[10] Park EJ, Kim H, Kim Y, Yi J, Choi K, Park K. Carbon fullerenes (C60s) can induce inflammatory responses in the lung of mice. Toxicol Appl Pharmacol 2010; 244(2):226–33.
[11] Poland CA, Duffin R, Kinloch I, Maynard A, Wallace WA, Seaton A, et al. Carbon nanotubes introduced into the abdominal cavity of mice show asbestos-like pathogenicity in a pilot study. Nat Nanotechnol 2008;3(7):423–8.
[12] Shin JA, Lee EJ, Seo SM, Kim HS, Kang JL, Park EM. Nanosized titanium dioxide enhanced inflammatory responses in the septic brain of mouse. Neuroscience 2010;165(2):445–54.
[13] Takagi A, Hirose A, Nishimura T, Fukumori N, Ogata A, Ohashi N, et al. Induction of mesothelioma in p53+/– mouse by intraperitoneal application of multi-wall carbon nanotube. J Toxicol Sci 2008;33(1):105–16.
[14] Yamashita K, Yoshioka Y, Higashisaka K, Morishita Y, Yoshida T, Fujimura M, et al. Carbon nanotubes elicit DNA damage and inflammatory response relative to their size and shape. Inflammation 2010;33(4):276–80.
[15] Nabeshi H, Yoshikawa T, Matsuyama K, Nakazato Y, Arimori A, Isobe M, et al. Size-dependent cytotoxic effects of amorphous silica nanoparticles on Langerhans cells. Pharmazie 2010;65(3):199–201.
[16] Singh S, Shi T, Duffin R, Albrecht C, van Berlo D, Hohr D, et al. Endocytosis, oxidative stress and IL-8 expression in human lung epithelial cells upon

treatment with fine and ultrafine $TiO_2$: role of the specific surface area and of surface methylation of the particles. Toxicol Appl Pharmacol 2007;222 (2):141–51.
[17] Thibodeau M, Giardina C, Hubbard AK. Silica-induced caspase activation in mouse alveolar macrophages is dependent upon mitochondrial integrity and aspartic proteolysis. Toxicol Sci 2003;76(1):91–101.
[18] Chlopek J, Czajkowaska B, Szaraniec B, Frackowiak E, Szostak K, Beguin F. *In vitro* studies of carbon nanotubes biocompatibility. Carbon 2006;44:1106–11.
[19] Bharali DJ, Klejbor I, Stachowiak EK, Dutta P, Roy I, Kaur N, et al. Organically modified silica nanoparticles: a nonviral vector for *in vivo* gene delivery and expression in the brain. Proc Natl Acad Sci U S A 2005;102(32):11539–44.
[20] Bottini M, D'Annibale F, Magrini A, Cerignoli F, Arimura Y, Dawson MI, et al. Quantum dot-doped silica nanoparticles as probes for targeting of T-lymphocytes. Int J Nanomedicine 2007;2(2):227–33.
[21] Hirsch LR, Stafford RJ, Bankson JA, Sershen SR, Rivera B, Price RE, et al. Nanoshell-mediated near-infrared thermal therapy of tumors under magnetic resonance guidance. Proc Natl Acad Sci U S A 2003;100(23):13549–54.
[22] Roy I, Ohulchanskyy TY, Bharali DJ, Pudavar HE, Mistretta RA, Kaur N, et al. Optical tracking of organically modified silica nanoparticles as DNA carriers: a nonviral, nanomedicine approach for gene delivery. Proc Natl Acad Sci U S A 2005;102(2):279–84.
[23] Verraedt E, Pendela M, Adams E, Hoogmartens J, Martens JA. Controlled release of chlorhexidine from amorphous microporous silica. J Control Release 2010;142(1):47–52.
[24] Ames BN, Gurney EG, Miller JA, Bartsch H. Carcinogens as frameshift mutagens: metabolites and derivatives of 2-acetylaminofluorene and other aromatic amine carcinogens. Proc Natl Acad Sci U S A 1972;69(11):3128–32.
[25] Ames BN, Durston WE, Yamasaki E, Lee FD. Carcinogens are mutagens: a simple test system combining liver homogenates for activation and bacteria for detection. Proc Natl Acad Sci U S A 1973;70(8):2281–5.
[26] McCann J, Spingarn NE, Kobori J, Ames BN. Detection of carcinogens as mutagens: bacterial tester strains with R factor plasmids. Proc Natl Acad Sci U S A 1975;72(3):979–83.
[27] Mortensen LJ, Oberdorster G, Pentland AP, Delouise LA. *In vivo* skin penetration of quantum dot nanoparticles in the murine model: the effect of UVR. Nano Lett 2008;8(9):2779–87.
[28] Nohynek GJ, Lademann J, Ribaud C, Roberts MS. Grey goo on the skin? Nanotechnology, cosmetic and sunscreen safety. Crit Rev Toxicol 2007;37(3): 251–77.
[29] Wolf R, Matz H, Orion E, Lipozencic J. Sunscreens–the ultimate cosmetic. Acta Dermatovenerol Croat 2003;11(3):158–62.
[30] AshaRani PV, Low Kah Mun G, Hande MP, Valiyaveettil S. Cytotoxicity and genotoxicity of silver nanoparticles in human cells. ACS Nano 2009;3(2): 279–90.
[31] Akey CW. Interactions and structure of the nuclear pore complex revealed by cryo-electron microscopy. J Cell Biol 1989;109(3):955–70.
[32] Reichelt R, Holzenburg A, Buhle Jr EL, Jarnik M, Engel A, Aebi U. Correlation between structure and mass distribution of the nuclear pore complex and of distinct pore complex components. J Cell Biol 1990;110(4):883–94.
[33] European Centre for Ecotoxicology and Toxicology of Chemicals (ECETOC). Synthetic Amorphous Silica (CAS No. 7631-86-9). ECETOC JACC Report No.51; 2006.
[34] Enterline PE, Henderson V. Type of asbestos and respiratory cancer in the asbestos industry. Arch Environ Health 1973;27(5):312–7.
[35] Luo S, Liu X, Mu S, Tsai SP, Wen CP. Asbestos related diseases from environmental exposure to crocidolite in Da-yao, China. I. Review of exposure and epidemiological data. Occup Environ Med 2003;60(1):35–42.
[36] McDonald JC, McDonald AD. The epidemiology of mesothelioma in historical context. Eur Respir J 1996;9(9):1932–42.
[37] Selikoff IJ, Lilis R, Nicholson WJ. Asbestos disease in United States shipyards. Ann N Y Acad Sci 1979;330:295–311.

Nabeshi et al. Particle and Fibre Toxicology 2011, 8:1
http://www.particleandfibretoxicology.com/content/8/1/1

PARTICLE AND FIBRE TOXICOLOGY

RESEARCH Open Access

# Amorphous nanosilica induce endocytosis-dependent ROS generation and DNA damage in human keratinocytes

Hiromi Nabeshi[1,2], Tomoaki Yoshikawa[1,2*], Keigo Matsuyama[1,2], Yasutaro Nakazato[1,2], Saeko Tochigi[1,2], Sayuri Kondoh[1,2], Toshiro Hirai[1,2], Takanori Akase[1,2], Kazuya Nagano[2], Yasuhiro Abe[2], Yasuo Yoshioka[2,3], Haruhiko Kamada[2,3], Norio Itoh[1], Shin-ichi Tsunoda[1,2,3], Yasuo Tsutsumi[1,2,3*]

## Abstract

**Background:** Clarifying the physicochemical properties of nanomaterials is crucial for hazard assessment and the safe application of these substances. With this in mind, we analyzed the relationship between particle size and the *in vitro* effect of amorphous nanosilica (nSP). Specifically, we evaluated the relationship between particle size of nSP and the *in vitro* biological effects using human keratinocyte cells (HaCaT).

**Results:** Our results indicate that exposure to nSP of 70 nm diameter (nSP70) induced an elevated level of reactive oxygen species (ROS), leading to DNA damage. A markedly reduced response was observed using submicron-sized silica particles of 300 and 1000 nm diameter. In addition, cytochalasin D-treatment reduced nSP70-mediated ROS generation and DNA damage, suggesting that endocytosis is involved in nSP70-mediated cellular effects.

**Conclusions:** Thus, particle size affects amorphous silica-induced ROS generation and DNA damage of HaCaT cells. We believe clarification of the endocytosis pathway of nSP will provide useful information for hazard assessment as well as the design of safer forms of nSPs.

## Background

With recent developments in nanotechnology, various kinds of nanomaterials have been designed and produced throughout the world. Nanomaterials have been widely used in consumer and industrial applications, such as medicine, cosmetics and foods, because they exhibit unique physicochemical properties and innovative functions [1]. For example, materials such as amorphous silica nanoparticles (nSPs) and titanium dioxide ($TiO_2$) are colorless and reflect ultraviolet light more efficiently than micro-sized particles. Consequently, these substances are already used as functional ingredients in many cosmetics such as foundation creams and sunscreens.

However, concerns over the potentially harmful effects of nanomaterials have been raised precisely because they possess novel properties that are different from those of microsized materials. Increasing numbers of studies show that many types of nanomaterials, such as carbon nanotubes, fullerenes, quantum dots, zinc oxide and $TiO_2$, have a harmful effect on cells and rodents [2-14]. For example, previous studies reported that various nanoparticles induced toxicological effects mainly in lung, liver, spleen and kidney tissues [3,10,15-19]. *In vivo* toxicity studies in Sprague Dawley rats showed that inhaled silver nanoparticles elicited chronic inflammation in the lungs [20]. After intravenous injection with silica nanoparticles in BALB/c mice, 70 nm particles induced liver injury at 30 mg/kg, while 300 nm or 1000 nm had no effect [21]. Recent evidence indicates that the small size and high surface area of nanomaterials may cause unpredictable genotoxic properties [22]. For example, induction of DNA damage by gold-, silver-, cobalt-, $TiO_2$-nanoparticles has been reported. The results from various studies suggest that these nanomaterials may cause DNA damage by an indirect pathway through promoting oxidative stress and inflammatory responses *via* dysfunction of

* Correspondence: tomoaki@phs.osaka-u.ac.jp; ytsutsumi@phs.osaka-u.ac.jp
[1]Graduate School of Pharmaceutical Sciences, Osaka University, 1-6 Yamadaoka, Suita, Osaka 565-0871, Japan
Full list of author information is available at the end of the article

mitochondria or inflammasomes. Central to the study of nanotoxicology is genotoxicity, the study of genetic aberrations following exposure to nanomaterials, because it is known that an increased genetic instability is associated with the development of cancer.

A sufficient understanding of the relationship between the physicochemical characteristics of nanomaterials governing their cytotoxicity (i.e. genotoxicity) and the identification of factors that influence their associated hazards are essential for the development of safer nanomaterials [22-25]. Since the linkage analysis is the sole methods for developing safe nanomaterials, many researchers have conducted extensive efforts [26-30]. In this context, the aim of our study was to investigate the relationship between particle size and in vitro hazard of amorphous nanosilica (nSP), especially focusing on DNA damage, using human keratinocyte cells.

## Results and Discussion

We first analyzed the physicochemical properties of the commercially available silica particles of 70, 300 and 1000 nm in diameter (nSP70, nSP300 and mSP1000, respectively). Close examination of the silica particles of different particle sizes (nSP70, nSP300, mSP1000) by scanning electron microscopy (SEM) revealed that all the particles used in this study were spherical and the primary particle sizes were approximately uniform (Figure 1A-C). The size distribution spectrum of each set of silica particles in a neutral solvent showed a single peak. Moreover, the average particle size corresponded almost precisely to the anticipated size for each sample (Figure 1D and 1E). These results suggest that the silica particles used in this study remained as stable well-dispersed particles in solution.

Cosmetic products containing nSP, such as those used in skincare treatments, have been on the market

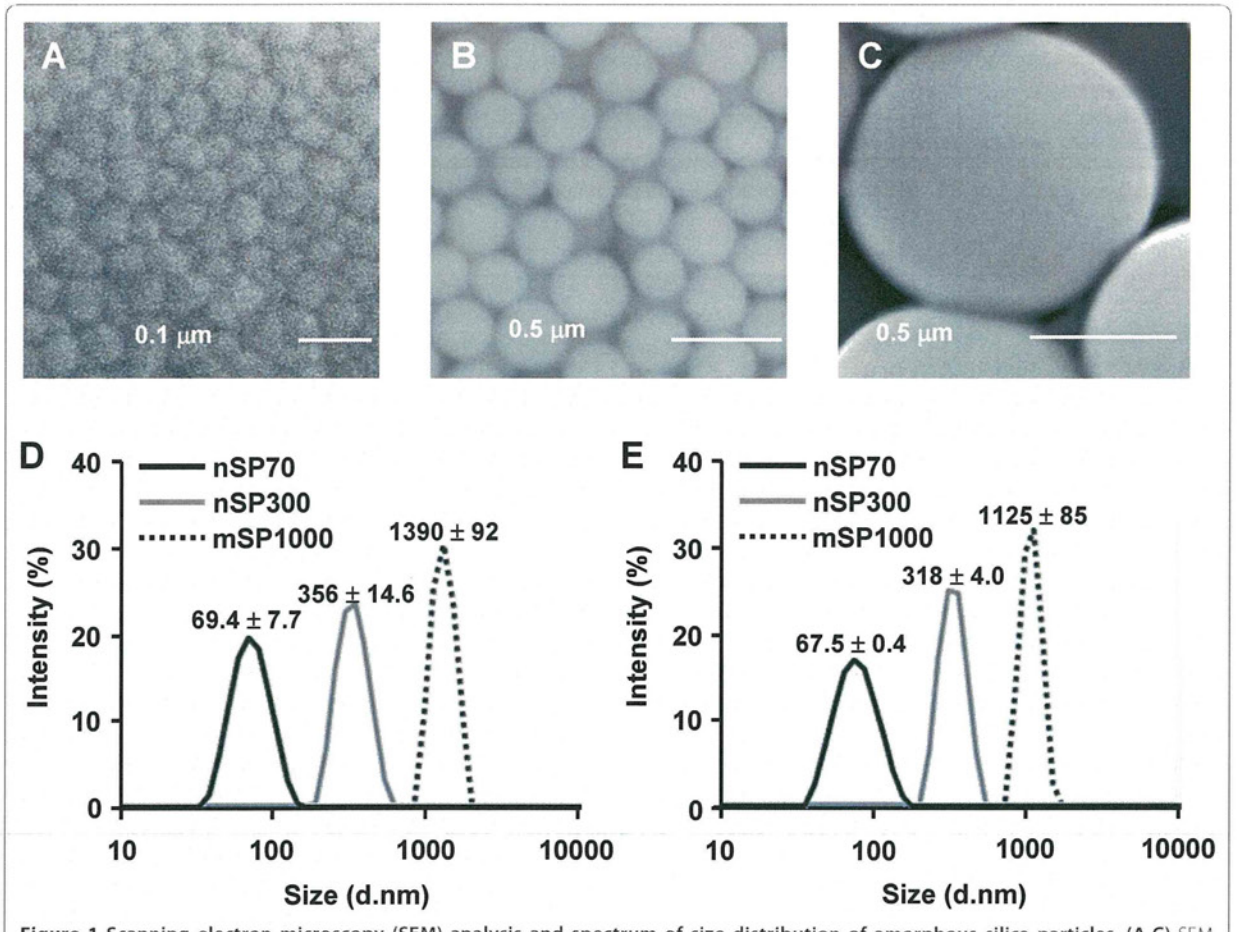


**Figure 1 Scanning electron microscopy (SEM) analysis and spectrum of size distribution of amorphous silica particles.** **(A-C)** SEM photomicrographs of silica particles used in this study: nSP70 (**A**), nSP300 (**B**) and mSP1000 (**C**). Scale bars: 0.1 mm (**A**) and 0.5 mm (**B and C**). **(D and E)** Size distribution of nSP70 (black), nSP300 (gray) and mSP1000 (dashed line) in water (**D**) or PBS (**E**) were measured by a dynamic light scattering method.

for a considerable period of time. Adult human skin has an average surface area of 1.95 $m^2$, weighs 3.18 kg and comprises over 300 million cells. The skin is the largest organ in the human body, which provides protection against heat, cold, electromagnetic radiation and chemical damage. Indeed, skin cells are likely to have the highest frequency of exposure to nSPs. Hence, a safety evaluation of nSPs using dermal cells is essential. Based on this consideration, using the HaCaT human keratinocyte cell line as a model system, we studied the effects of various sized silica particles on cell function. Specifically, we used HaCaT cells to perform the LDH release assay to assess membrane damage induced by silica particles. We found that membrane damage was not observed in nSP300- and mSP1000-treated HaCaT cells. By contrast, LDH release increased after exposure of the cells to nSP70 in a dose-dependent manner (Figure 2). This observation suggested that membrane damage in keratinocytes increased significantly when the particle size was less than 100 nm. The decrease of particle size changes the physicochemical properties of the silica particles, such as surface area and the number of functional groups per particle weight, which are both increased [31-34]. In addition, subsequent experiments were performed at a non-toxic dose (less than 300 μg/ml) in order to exclude the toxic effects of nSP70.

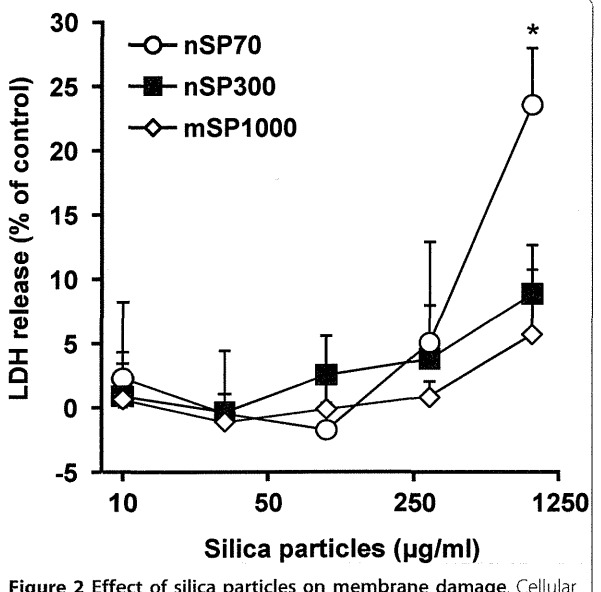


**Figure 2 Effect of silica particles on membrane damage.** Cellular membrane damage in HaCaT cells after incubation with nSP70 (circles), nSP300 (squares) and mSP1000 (diamonds) for 24 h was evaluated by the LDH release assay. The percentage cellular membrane damage was calculated relative to the negative (medium) controls. Data are presented as means ± SD (n = 3).*$P$ < 0.01 vs same dose of nSP300 and mSP1000.

Some reports have indicated that intracellular generation of reactive oxygen species (ROS) is induced by nSP [35-37]. Furthermore, it has recently been reported that crystalline silica induces intracellular ROS generation *via* NADPH oxidase activation following uptake by endocytosis [38,39]. Based on these reports, ROS generation and DNA damage are an obvious means of assessing the hazard posed by nSP. Firstly, total intracellular ROS generation was measured in silica particle-treated HaCaT cells using 2'7'-dichlorodihydorofluorescein diacetate (DCFH-DA). Silica particles of all sizes were found to induce intracellular ROS generation in a dose-dependent fashion (Figure 3A). However, ROS generation by nSP70 treatment was significantly greater compared with nSP300 and mSP1000 treatment at the same particle concentration. Additionally, we confirmed that hydroxyl radicals, one of the most highly reactive ROS, were generated in HaCaT cells treated with silica particles, in particular with nSP70 (Figure 3B). Even in the 10 μg/ml-treated group, hydroxyl radical-generation effects of nSP70-treatment were 1.4 times higher than that of nSP300 and mSP1000-treated groups. These results suggested that silica particle-induced intracellular ROS generation was significantly increased by decreasing the particle size to less than 100 nm. ROS are defined as either "primary" or "secondary". Primary ROS (e.g. superoxide, $O_2^-$) can be generated through metabolic processes or through the activation of oxygen, which results in the formation of a reactive nucleophilic molecule of oxygen i.e., superoxide anion. These reactive species may interact with other molecules, such as redox active transition metals (e.g. iron) or enzymes, resulting in the production of "secondary" ROS (e.g. $^{\bullet}OH$), which are primary mediators of DNA damage. Consequently, we analyzed the formation of 7'8'-dihydro-8-oxodeoxyguanosine (8-OH-dG) as an indicator of ROS-induced DNA damage. When HaCaT cells were treated with various concentrations of silica particles for 3 h, 8-OH-dG levels in nSP300- and mSP1000-treated cells remained constant regardless of silica particle dose and were equal to the levels found in untreated cells (Figure 3C). By contrast, 8-OH-dG levels increased upon exposure of the cells to nSP70 in a dose-dependent manner. After treatment with nSP70 at 90 μg/ml the level of 8-OH-dG increased significantly compared with non-treated cells.

8-OH-dG is known as a major index of oxidative DNA damage related to mutagenesis, carcinogenesis and the aging process [40,41]. These reports, together with our results, suggest the possibility that nSP70 may be carcinogenic. Moreover, nSP-induced ROS may induce genotoxicity *via* DNA strand breaks, oxidative DNA damage and mutation. Indeed, DNA damage was detected in nSP70-treated HaCaT cells. In addition, nSP70-mediated DNA damage was inhibited by pre-treatment with the ROS scavenger, N-acetylcystein

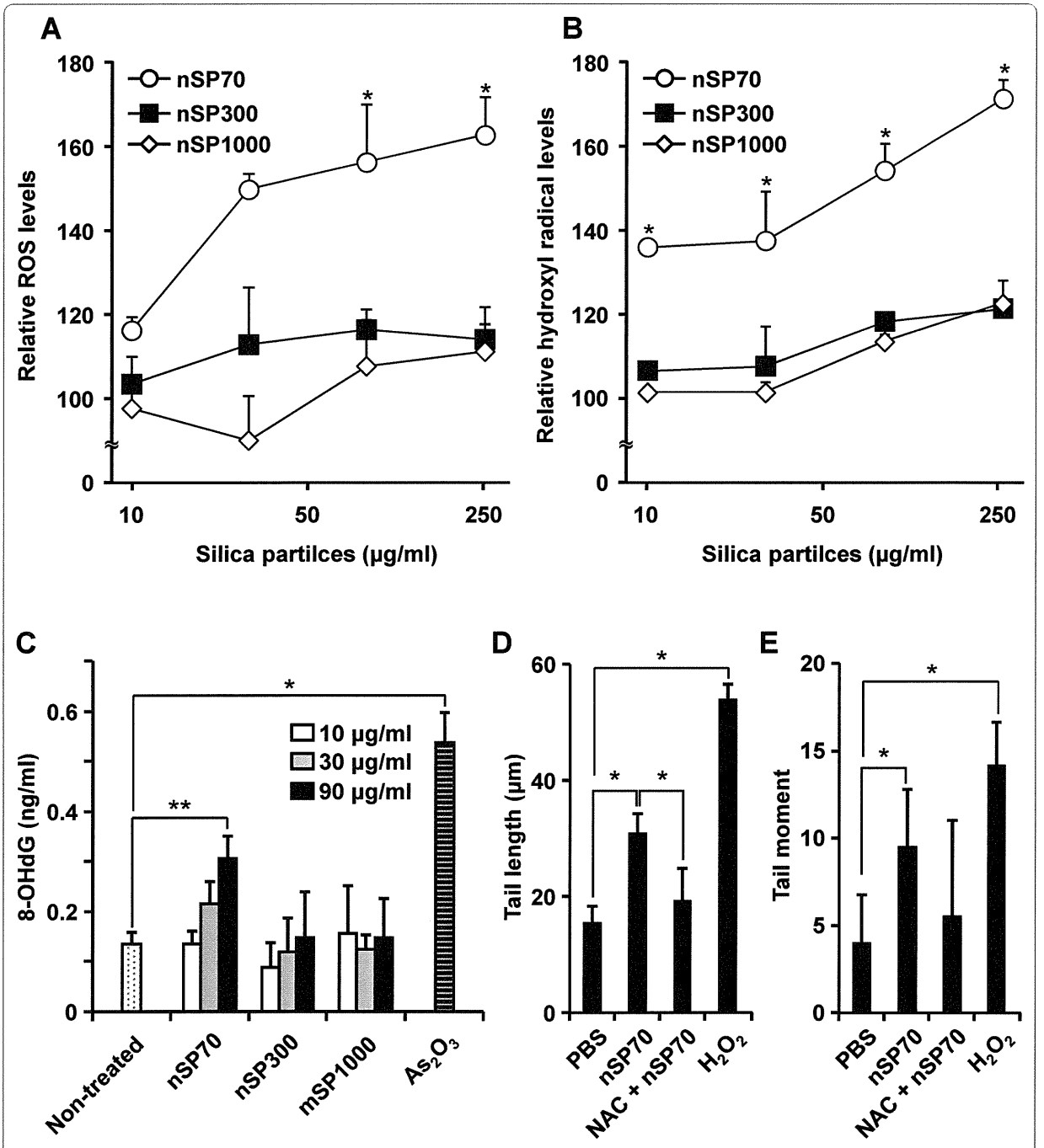


**Figure 3 Detection of oxidative stress induced by silica particle treatment in HaCaT cells**. Detection of total ROS and hydroxyl radical induced by silica particle treatment in HaCaT cells. HaCaT cells were incubated with various concentrations of nSP70 (circles), nSP300 (squares), and mSP1000 (diamonds) for 3 h. (**A**) Total ROS induced by treatment with silica particles were expressed as relative fluorescence units in the DCFH assay.*$P < 0.01$ vs same dose of nSP300 and mSP1000. (**B**) Hydroxyl radical was measured by hydroxyphenyl fluorescein (HPF) assay. Data shown are means ± SD (n = 3).*$P < 0.01$ vs same dose of nSP300 and mSP1000. (**C**) Detection of 8-OH-dG induced by silica particle treatment in HaCaT cells. HaCaT cells were incubated with 10, 30 or 90 mg/ml nSP70, nSP300, or mSP1000, and $As_2O_3$ (positive control) for 3 h. Data shown are means ± SD (n = 3). *$P < 0.01$, **$P < 0.05$. (**D and E**) Effects of ROS inhibitor on DNA strand breaks induced by silica particle treatment in HaCaT cells. HaCaT cells were pretreated with 2 mM N-acetylcystein (NAC) for 30 min (NAC + nSP70) or nSP70 alone, prior to incubation with 90 mg/ml nSP70 for 3 h. As a positive control, HaCaT cells were treated with 0.2 mM $H_2O_2$ for 3 h. (**D**) Column height shows the tail length. (**E**) Column height shows the tail moment. Data shown are means ± SD of at least 16 cells per sample. Results shown are representative of more than three independent experiments. *$P < 0.01$.

(NAC) (Figure 3D and 3E). From the results of the present study, we suggest that ROS play an important role in cellular responses such as nSP-induced DNA damage. However, the reason why ROS generation varies with particle size has not yet been clarified.

Fine or ultrafine particulate matter (PM), such as diesel exhaust particles or crystalline silica, often induces ROS generation that contributes to the induction of DNA damage or apoptosis. Although the mechanisms underlying the PM-induced oxidative stress response remains unclear, strong evidence supports PM phagocytosis as a stimulus for increased oxidative stress *via* NADPH oxidase activation [38,42,43]. In addition, Walee Chamulitrat *et al.* reported that HaCaT cells constitutively express Nox components Rac1, p40phox, and p67phox proteins [44]. In HaCaT skin keratinocyte cells, stimuli such as epidermal growth factor, $Ca^{2+}$-ionophore A23187, lysophosphatidic acid are capable of producing ROS [45-47]. Thus, one potential candidate for the nSP70-mediated DNA damage is ROS, which is produced by NADPH oxidase upon nSP70 phagocytosis. In order to assess the relationship between the uptake pathway and ROS generation, we measured the production of ROS induced by nSP70 in the presence or absence of a specific inhibitor of endocytosis. After treatment with cytochalasin D, an inhibitor of actin polymerization [48], ROS generation induced by nSP70 was measured by DCFH-DA assay. Results indicated that ROS generation induced by nSP70 was inhibited by pretreatment with cytochalasin D in a dose-dependent manner (Figure 4). Furthermore, nSP70-induced DNA damage was also significantly reduced by pretreatment with cytochalasin D (Figure 5A and 5B). These findings suggest that the silica particles entered the cells mainly through actin-mediated endocytosis, such as the macropinocytosis pathway, thereby inducing ROS generation and DNA damage. It is well-known that NADPH oxidase, which exists in the cytosol, cellular membrane and subcellular compartment membranes, becomes activated and generates ROS after ingestion of microorganisms into the phagosome and/or endosome [49-51]. Moreover, it is reported that $TiO_2$ particles induce IL-1ß production by NADPH oxidase-mediated ROS generation in the human macrophage cell line [52]. Likewise, NADPH oxidase exists in the cytosol and membranes of non-phagocyte cells, including HaCaT cells [44]. Additionally, it had been reported that inflammasomes are activated by actin-mediated endocytosis of crystalline silica, which lead to NADPH oxidase activation and ROS generation [38,39,53]. Consequently, in order to determine the role of NADPH oxidase in silica particle-induced ROS generation, the effects of pretreatment with the NADPH oxidase inhibitor, apocynin, a well-known NOX inhibitor [49,54], were investigated. As

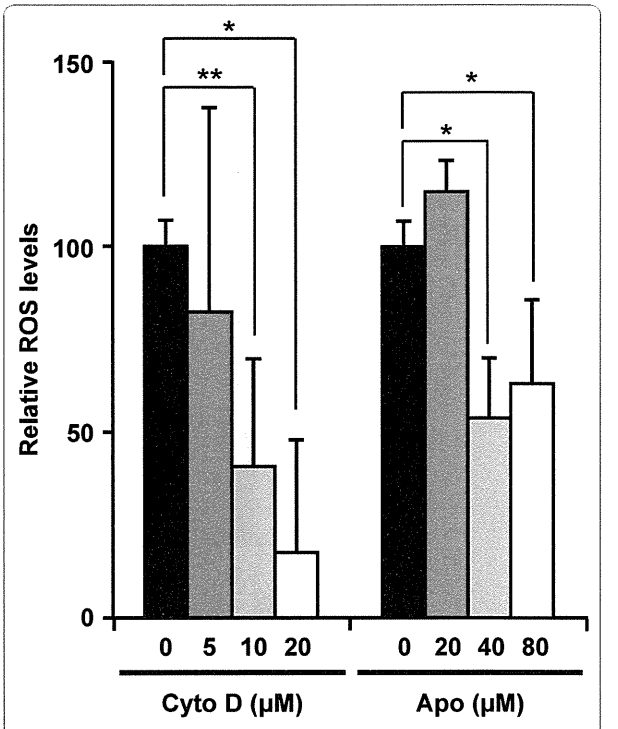


**Figure 4 Effects of endocytosis and NADPH oxidase inhibitor on generation of ROS induced by silica particle treatment.** HaCaT cells were pretreated with cytochalasin D or apocynin for 30 min prior to incubation with 270 mg/ml nSP70 for 3 h. ROS induced by silica particle treatment were expressed as relative fluorescence units, which means that ROS intensity of each silica particle alone and non-treatment is 100 and 0 respectively, in the DCFH assay. Data shown are means ± SD (n = 3). $^{*}P < 0.01$, $^{**}P < 0.05$.

expected, nSP70-induced ROS generation was inhibited in the presence of apocynin (Figure 4). In contrast, DNA damage induced by nSP70 was not inhibited by pretreatment with apocynin (Figure 5C and 5D). Taken together, these results suggest that nSP70-mediated DNA damage was induced by ROS generated by an unknown mechanism, and not *via* NADPH oxidase. Nox1 activation may initiate large bursts of ROS that can mediate the killing of pathogens, such as *H. pylori* [55]. Thus, NOX1 activation has been implicated in the cutaneous innate immunity to bacterial infections of the skin. A more detailed evaluation of the mechanism that underlies nSP70-mediated NOX activation is essential. Nonetheless, based on our results and the work of others, we speculate that nSP70s are treated almost like pathogens by HaCaT cells.

A number of mechanisms underlie the ability of nanoparticles to cause DNA damage. As mentioned above, a key mechanism that is often described is the ability of particles to cause the production of ROS [32,56]. One possible mechanism of particle-mediated DNA damage

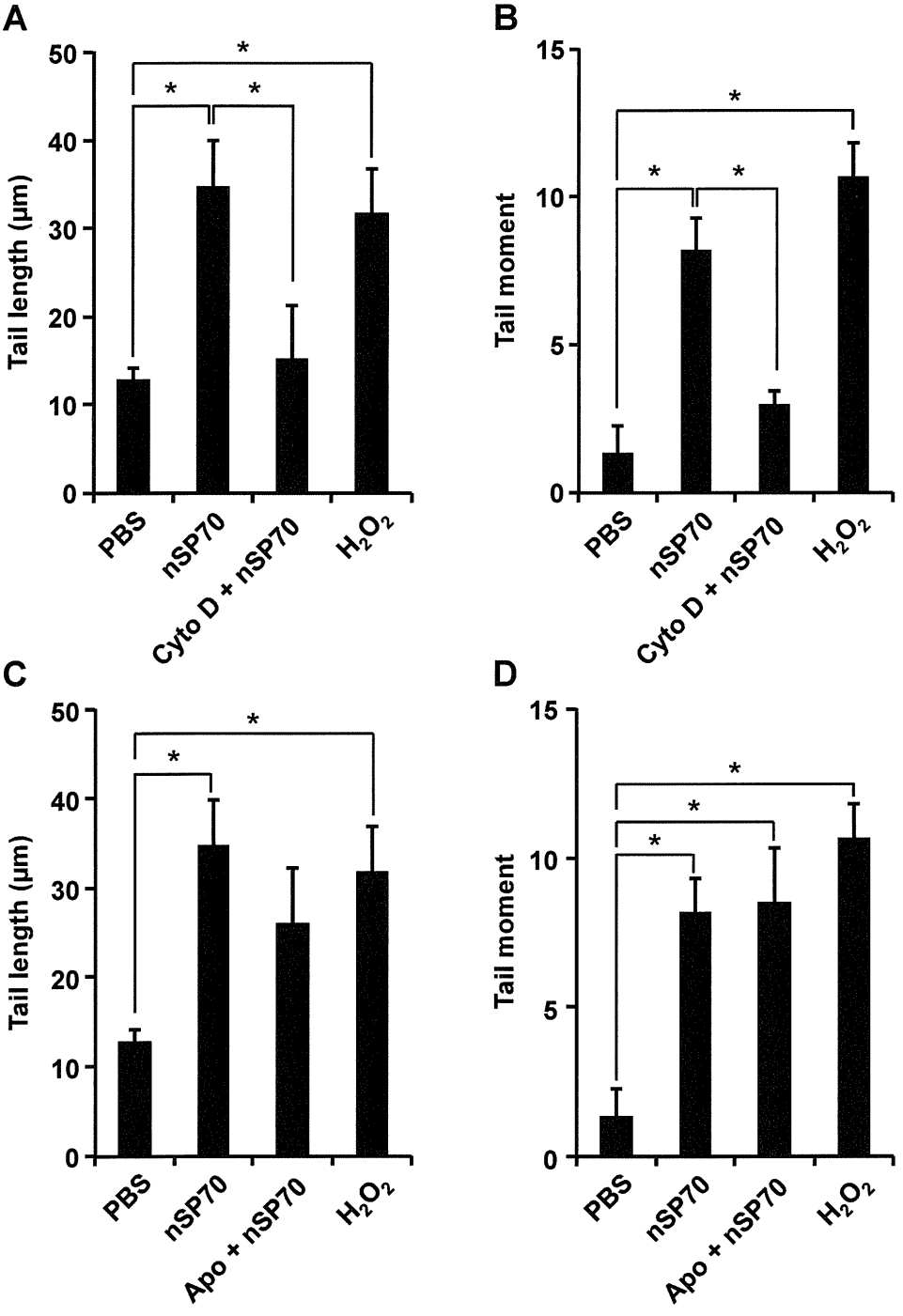


**Figure 5 Effects of endocytosis and NADPH oxidase inhibitor on DNA damage by silica particle treatment**. Effects of endocytosis inhibitor (**A and B**) or NADPH oxidase inhibitor (**C and D**) on DNA strand breaks induced by silica particle treatment in HaCaT cells. (**A and B**) HaCaT cells were pretreated with 10 mM cytochalasin D (Cyto D) for 30 min (Cyto D + nSP70) or nSP70 alone, prior to incubation with 90 mg/ml nSP70 for 3 h. (**C and D**) HaCaT cells were pretreated with 40 mM apocynin (Apo) for 30 min (Apo + nSP70) or nSP70 alone, prior to incubation with 90 mg/ml nSP70 for 3 h. As a positive control, HaCaT cells were treated with 0.2 mM $H_2O_2$ for 3 h. (**A and C**) Column height shows the tail length. (**B and D**) Column height shows the tail moment. Data shown are means ± SD of at least 16 cells per sample. Results shown are representative of more than three independent experiments. *$P < 0.01$.

is the ability of particles to stimulate target cells to produce oxidants/genotoxic compounds e.g., by affecting mitochondrial electron transport, activation of NADPH oxidase, or inducing cytochrome P450 enzymes. Our results show that nSP70-mediated DNA damage of HaCaT cells occurred *via* a mechanism that did not involve NADPH oxidase. Alternatively, transition metal ions (such as cadmium, chromium, cobalt, copper, iron, nickel, titanium and zinc) released from certain nanoparticles have the potential to cause the conversion of cellular oxygen metabolic products such as $H_2O_2$ and superoxide anions to hydroxyl radicals, which is one of the primary DNA damaging species. Well-known examples of the consequences of metal ion-contamination in relation to nanotoxicity have been described for carbon nanotubes. Indeed, iron contaminants in CNT have been shown to result in a substantial loss of glutathione and increased lipid peroxidation in alveolar macrophages, indicators of oxidative stress [57]. However, our data suggests that the nSPs used in this study, nSP70, nSP300 and mSP1000, were not contaminated with metal ions (data not shown). Thus, it is highly unlikely that metal ion contamination is involved in nSP70-induced DNA damage. Another hypothesis is that the size of nSPs is related to its oxidative stress. As particle size decreases, the particle unit of mass and overall surface area increases. This larger surface area enhances catalytic activity. Indeed, it has been widely reported that increased surface area of these particles increases reactivity because surface atoms have a tendency to possess high energy bonds. In order to gain stabilization, these surface bonds will readily react with other molecules [58]. The specific surface area was calculated by means of the following equation; $s = 6/d\rho$ (where s, specific surface area ($m^2/g$); $\rho$, density (g/cc); d, diameter ($\mu m$)). The specific surface area of nSP70, nSP300 and mSP1000 calculated using this equation was 43, 10 and 3 $m^2/g$, respectively. When specific area is considered, rather than particle concentration, the membrane damage activity of nSP70 and nSP300-treated cells shows almost the same level of LDH release per unit surface area (data not shown). In terms of ROS generation and DNA oxidation, nSP70 is more potent than nSP300. These results suggest that nSP70, which possesses a larger specific surface area compared to the counterpart micron-sized silica particles, has a much greater chance of interaction with biomolecules. Consequently, nSP70 causes direct cellular damage and promotion of oxidative stress. In addition to these hypotheses, nanoparticles may gain direct access to DNA *via* nuclear transport. However, this mechanism seems very unlikely given that the nuclear pore complex is known to be 8-30 nm in diameter, depending on cell type [59]. Nonetheless, some studies have reported that nanoparticles can penetrate the nuclear membrane, such as silica nanoparticles (40-70 nm) [60]. Detailed analysis of the mechanism of DNA damage induced by nanoparticles is currently underway. This information will be a critical determinant in the design of safer nSPs and will provide valuable information for hazard assessment of nSPs.

Here, we report the effects induced by well-dispersed amorphous silica particles (nSPs) on human keratinocyte (HaCaT) cells. In addition to our own work, other studies have shown that well-dispersed nSPs induce cytotoxicity, including LDH release, in a dose-dependent and size-dependent manner using a macrophage cell line [61,62]. On the other hands, Lin et al. reported that nSPs mediated cytotoxicity/DNA damage against A549 cells were not correlated with particle size [36]. Further, Barnes et al. reported that nSP induce no genotoxicity in fibroblast 3T3-L1 cells [63]. From the viewpoint of nSP-mediated toxicity, there is no consistency in these four reports including our findings. As mentioned above, there are a number of examples in the literature of conflicting results regarding nSPs. It has becoming increasingly evident that the physicochemical properties of nanomaterials, such as the size, shape, surface charge, fabricating method, etc, play a central role in governing their cellular uptake and subsequent physiologic consequences. Furthermore, experimental conditions, such as cell type and incubation time, are critical for the nanotoxicologic studies. Hence, given the inconsistencies it is difficult to draw the same conclusions. However, our results using well-dispersed nSPs indicated that nSPs were more cytotoxic and genotoxic against the human keratinocyte cell line HaCaT.

## Conclusions

In this study, we show that nSP induce certain cellular responses, such as ROS generation and DNA damage. By contrast, their bulk-sized counterparts display a much reduced response. These different responses might be partly due to different mechanisms, such as intracellular uptake and ROS generation. We speculated that receptor-mediated uptake was involved in these phenomena and set out to identify the physicochemical properties that affect receptor endocytosis. We believe a detailed analysis of nSP-internalization will be invaluable for both hazard assessment and the design of safe nSPs.

## Materials and methods

### Silica particles

Suspensions of fluorescent (red-F)-labeled amorphous silica particles (Micromod Partikeltechnologie GmbH) (25 mg/ml and 50 mg/ml) were used in this study; particle size diameters were 70, 300 and 1000 nm (designated as nSP70, nSP300 and mSP1000,

respectively). Silica particle suspensions were stored in the dark at room temperature. The suspensions were sonicated for 5 min and then vortexed for 1 min immediately prior to use.

### Cell Culture

The HaCaT human keratinocyte cell line was kindly provided by Dr. Inui [64], Osaka University. HaCaT cells were cultured in Dulbecco's modified Eagle's medium (D-MEM) supplemented with 10% heat-inactivated fetal bovine serum and 0.2 mM L-glutamine. The cells were grown in a humidified incubator at 37°C (95% room air, 5% $CO_2$).

### Physicochemical examinations of silica particles

Silica particle suspensions were diluted to 0.25 mg/ml (nSP70), 0.5 mg/ml (nSP300 and mSP1000) with water or PBS, respectively and the average particle sizes were then measured using the Zetasizer Nano-ZS (Malvern Instruments Ltd). The mean size and the size distribution of silica particles were measured by a dynamic light scattering method. The size and shape of silica particles were determined using scanning electron microscopy (SEM). Each silica particle suspension was dropped on the sample stage and dried. The dried silica particles were then observed by SEM.

### LDH release assay

Lactate dehydrogenase (LDH) is released from HaCaT cells exposed to nSP70, nSP300 or mSP1000. The LDH activity of the supernatant of the culture medium was determined using a commercial LDH cytotoxicity test (WAKO, Japan) according to the manufacturer's instructions. In brief, $5 \times 10^3$ cells were seeded into each well of a 96-well plate. After 24 h incubation, cells were treated with nSP70, nSP300, mSP1000 or 0.2% Tween 20 (positive control). After a further 24 h incubation period, 50 μl of medium overlying cells was used for LDH analysis. Absorption of light at 560 nm was measured using a spectrophotometer.

### Detection of Reactive Oxygen Species (ROS)

The generation of total intracellular ROS was measured by monitoring the increasing fluorescence of 2'7'-dichlorofluorescein (DCF). The cell-permeant 2'7'-dichlorodihydorofluorescein diacetate (DCFH-DA; Sigma, St. Louis, MO) enters the cell where intracellular esterases cleave off the diacetate group. The resulting DCFH is retained in the cytoplasm and oxidized to DCF by ROS. Hydroxyl radical was measured by monitoring the increasing fluorescence of hydroxyphenyl fluorescein (HPF; SEKISUI MEDICAL Co., Ltd., Japan). $3 \times 10^4$ HaCaT cells were seeded into each well of a 96-well plate. After 24 h incubation, cells were treated with nSP70, nSP100, nSP300, mSP1000 or 2 mM $H_2O_2$ (positive control). Cells were then washed once with phenol red-free medium, and incubated in 100 μl working solution of DCFH-DA or HPF (10 μM) at 37°C for 30 min. Using the fluorescence reader (ARVO MX; Perkin Elmer, Waltham, MA), the fluorescence of DCF or HPF was monitored at the excitation and emission wavelengths of 485 nm and 530 nm or 490 nm and 515 nm, respectively.

### 8-Hydroxy-2-deoxyguanosine (8-OH-dG) measurement

HaCaT cells were seeded on a 100 mm dish. After 24 h, cells were treated with various concentrations of nSP70, nSP300, mSP1000, 0.2 mM $H_2O_2$ (positive control) or PBS (negative control). After 3 h, cellular DNA was isolated using DNeasy tissue kit (QIAGEN, Germany). Ten μg of DNA was converted to single stranded DNA by incubation with 180 U Exonuclease III (Takara Biotech., Japan) at 37°C for 1 h. The DNA was heated at 95°C for 5 min, rapidly chilled on ice, and digested to nucleosides by incubation with 0.6 U nuclease P1 (Takara) at 37°C for 1 h followed by treatment with 0.6 U *E. coli* alkaline phosphatase (Takara) for a further 1 h. The reaction mixture was centrifuged (6000 × g for 1 min) and the supernatant used for the 8-OHdG assay. The amount of 8-OHdG was measured according to the protocol of the competitive ELISA kit (8-OHdG check; Japan Institute for the Control of Aging, Japan).

### Effects of inhibitor of ROS, endocytosis or NADPH oxidase on DNA strand breaks induced by silica particles

$3 \times 10^4$ HaCaT cells were pretreated with 2 mM N-acetylcystein (NAC, ROS scavenger), 10 mM cytochalasin D (endocytosis inhibitor) or 40 mM apocynin (NADPH oxidase inhibitor) for 30 min prior to incubation with 90 mg/ml of nSP70 for 3 h. As a positive control, HaCaT cells were treated with 0.2 mM $H_2O_2$ for 3 h. DNA strand breaks were detected by alkaline comet assay according to the Comet Assay Kit (Trevigen, Gaithersburg, MD). The samples were processed according to the protocol provided in the kit. Twenty-five cells on each slide, randomly selected by fluorescence microscopy, were then analyzed using the Comet Analyzer (Youworks Corporation, Japan).

### Effects of inhibitor of endocytosis, NADPH oxidase or endosomal acidification on generation of ROS induced by silica particles

HaCaT cells were pretreated with various concentration of cytochalasin D (Merck Ltd., Germany) for 30 min prior to incubation with 270 mg/ml nSP70 for 3 h. ROS induced by treatment with silica particles were expressed as relative fluorescence units in the DCFH-DA assay as described above.

## Statistical analysis

Statistical comparisons between groups were performed by one-way ANOVA and a Bonferroni *post hoc* test. The level of significance was set at $P < 0.05$.

### Acknowledgements

This study was supported in part by Grants-in-Aid for Scientific Research from the Ministry of Education, Culture, Sports, Science and Technology of Japan, and from the Japan Society for the Promotion of Science (JSPS). This study was also supported in part by Health Labour Sciences Research Grants from the Ministry of Health, Labor and Welfare of Japan; by Health Sciences Research Grants for Research on Publicly Essential Drugs and Medical Devices from the Japan Health Sciences Foundation; by a Global Environment Research Fund from Minister of the Environment; and by a the Knowledge Cluster Initiative; and by Food Safety Commission; and by The Nagai Foundation Tokyo; and by The Cosmetology Research Foundation; and by The Smoking Research Foundation.

### Author details

[1]Graduate School of Pharmaceutical Sciences, Osaka University, 1-6 Yamadaoka, Suita, Osaka 565-0871, Japan. [2]Laboratory of Biopharamceutical Research (Pharmaceutical Proteomics), National Institute of Biomedical Innovation, 7-6-8, Saito-Asagi, Ibaraki, Osaka, 567-0085, Japan. [3]The Center for Advanced Medical Engineering and Informatics, Osaka University, 1-6, Yamadaoka, Suita, Osaka, 565-0871, Japan.

### Authors' contributions

HN and TY designed the study. HN, KM, YN, STo, SK, TH and TA performed experiments. HN and TY collected and analysed data. HN and TY wrote the manuscript. KN, YA, YY, HK, NI and STs gave technical support and conceptual advice. YT supervised the all of projects. All authors discussed the results and commented on the manuscript.

### Competing interests

The authors declare that they have no competing interests.

Received: 13 September 2010 Accepted: 15 January 2011
Published: 15 January 2011

### References

1. Salata O: **Applications of nanoparticles in biology and medicine.** *J Nanobiotechnology* 2004, **2**:3.
2. Aiso S, Yamazaki K, Umeda Y, Asakura M, Takaya M, Toya T, Koda S, Nagano K, Arito H, Fukushima S: **Pulmonary Toxicity of Intratracheally Instilled Multiwall Carbon Nanotubes in Male Fischer 344 Rats.** *Ind Health* 2010.
3. Chen J, Dong X, Zhao J, Tang G: **In vivo acute toxicity of titanium dioxide nanoparticles to mice after intraperitioneal injection.** *J Appl Toxicol* 2009, **29**:330-337.
4. Geys J, Nemmar A, Verbeken E, Smolders E, Ratoi M, Hoylaerts MF, Nemery B, Hoet PH: **Acute toxicity and prothrombotic effects of quantum dots: impact of surface charge.** *Environ Health Perspect* 2008, **116**:1607-1613.
5. Heng BC, Zhao X, Xiong S, Ng KW, Boey FY, Loo JS: **Toxicity of zinc oxide (ZnO) nanoparticles on human bronchial epithelial cells (BEAS-2B) is accentuated by oxidative stress.** *Food Chem Toxicol* 2010, **48**:1762-1766.
6. Kocbek P, Teskac K, Kreft ME, Kristl J: **Toxicological Aspects of Long-Term Treatment of Keratinocytes with ZnO and TiO(2) Nanoparticles.** *Small* 2010, **6**:1908-1917.
7. Liu S, Xu L, Zhang T, Ren G, Yang Z: **Oxidative stress and apoptosis induced by nanosized titanium dioxide in PC12 cells.** *Toxicology* 2010, **267**:172-177.
8. Moos PJ, Chung K, Woessner D, Honeggar M, Cutler NS, Veranth JM: **ZnO particulate matter requires cell contact for toxicity in human colon cancer cells.** *Chem Res Toxicol* 2010, **23**:733-739.
9. Murray AR, Kisin E, Leonard SS, Young SH, Kommineni C, Kagan VE, Castranova V, Shvedova AA: **Oxidative stress and inflammatory response in dermal toxicity of single-walled carbon nanotubes.** *Toxicology* 2009, **257**:161-171.
10. Park EJ, Kim H, Kim Y, Yi J, Choi K, Park K: **Carbon fullerenes (C60s) can induce inflammatory responses in the lung of mice.** *Toxicol Appl Pharmacol* 2010, **244**:226-233.
11. Poland CA, Duffin R, Kinloch I, Maynard A, Wallace WA, Seaton A, Stone V, Brown S, Macnee W, Donaldson K: **Carbon nanotubes introduced into the abdominal cavity of mice show asbestos-like pathogenicity in a pilot study.** *Nat Nanotechnol* 2008, **3**:423-428.
12. Shin JA, Lee EJ, Seo SM, Kim HS, Kang JL, Park EM: **Nanosized titanium dioxide enhanced inflammatory responses in the septic brain of mouse.** *Neuroscience* 2010, **165**:445-454.
13. Takagi A, Hirose A, Nishimura T, Fukumori N, Ogata A, Ohashi N, Kitajima S, Kanno J: **Induction of mesothelioma in p53+/- mouse by intraperitoneal application of multi-wall carbon nanotube.** *J Toxicol Sci* 2008, **33**:105-116.
14. Yamashita K, Yoshioka Y, Higashisaka K, Morishita Y, Yoshida T, Fujimura M, Kayamuro H, Nabeshi H, Yamashita T, Nagano K, *et al*: **Carbon nanotubes elicit DNA damage and inflammatory response relative to their size and shape.** *Inflammation* 2010, **33**:276-280.
15. Chen Z, Meng H, Xing G, Chen C, Zhao Y, Jia G, Wang T, Yuan H, Ye C, Zhao F, *et al*: **Acute toxicological effects of copper nanoparticles in vivo.** *Toxicol Lett* 2006, **163**:109-120.
16. Duan Y, Liu J, Ma L, Li N, Liu H, Wang J, Zheng L, Liu C, Wang X, Zhao X, *et al*: **Toxicological characteristics of nanoparticulate anatase titanium dioxide in mice.** *Biomaterials* 2010, **31**:894-899.
17. Li JJ, Muralikrishnan S, Ng CT, Yung LY, Bay BH: **Nanoparticle-induced pulmonary toxicity.** *Exp Biol Med (Maywood)* 2010, **235**:1025-1033.
18. Li N, Duan Y, Hong M, Zheng L, Fei M, Zhao X, Wang J, Cui Y, Liu H, Cai J, *et al*: **Spleen injury and apoptotic pathway in mice caused by titanium dioxide nanoparticules.** *Toxicol Lett* 2010, **195**:161-168.
19. Liang G, Yin L, Zhang J, Liu R, Zhang T, Ye B, Pu Y: **Effects of subchronic exposure to multi-walled carbon nanotubes on mice.** *J Toxicol Environ Health A* 2010, **73**:463-470.
20. Sung JH, Ji JH, Yoon JU, Kim DS, Song MY, Jeong J, Han BS, Han JH, Chung YH, Kim J, *et al*: **Lung function changes in Sprague-Dawley rats after prolonged inhalation exposure to silver nanoparticles.** *Inhal Toxicol* 2008, **20**:567-574.
21. Nishimori H, Kondoh M, Isoda K, Tsunoda S, Tsutsumi Y, Yagi K: **Silica nanoparticles as hepatotoxicants.** *Eur J Pharm Biopharm* 2009, **72**:496-501.
22. Aillon KL, Xie Y, El-Gendy N, Berkland CJ, Forrest ML: **Effects of nanomaterial physicochemical properties on in vivo toxicity.** *Adv Drug Deliv Rev* 2009, **61**:457-466.
23. Hoshino A, Fujioka K, Oku T, Suga M, Sasaki FY, Ohta T, Yasuhara M, Suzuki K, Yamamoto K: **Physicochemical Properties and Cellular Toxicity of Nanocrystal Quantum Dots Depend on Their Surface Modification.** *Nano Letters* 2004, **4**:2163-2169.
24. Morishige T, Yoshioka Y, Inakura H, Tanabe A, Yao X, Narimatsu S, Monobe Y, Imazawa T, Tsunoda S, Tsutsumi Y, *et al*: **The effect of surface modification of amorphous silica particles on NLRP3 inflammasome mediated IL-1beta production, ROS production and endosomal rupture.** *Biomaterials* 2010, **31**:6833-6842.
25. Sohaebuddin SK, Thevenot PT, Baker D, Eaton JW, Tang L: **Nanomaterial cytotoxicity is composition, size, and cell type dependent.** *Part Fibre Toxicol* 2010, **7**:22.
26. Fourches D, Pu D, Tassa C, Weissleder R, Shaw SY, Mumper RJ, Tropsha A: **Quantitative nanostructure-activity relationship modeling.** *ACS Nano* 2010, **4**:5703-5712.
27. Puzyn T, Leszczynska D, Leszczynski J: **Toward the development of "nano-QSARs": advances and challenges.** *Small* 2009, **5**:2494-2509.
28. Shaw SY, Westly EC, Pittet MJ, Subramanian A, Schreiber SL, Weissleder R: **Perturbational profiling of nanomaterial biologic activity.** *Proc Natl Acad Sci USA* 2008, **105**:7387-7392.
29. Tropsha A, Golbraikh A: **Predictive QSAR modeling workflow, model applicability domains, and virtual screening.** *Curr Pharm Des* 2007, **13**:3494-3504.
30. Weissleder R, Kelly K, Sun EY, Shtatland T, Josephson L: **Cell-specific targeting of nanoparticles by multivalent attachment of small molecules.** *Nat Biotechnol* 2005, **23**:1418-1423.
31. Borm P, Klaessig FC, Landry TD, Moudgil B, Pauluhn J, Thomas K, Trottier R, Wood S: **Research strategies for safety evaluation of nanomaterials, part V: role of dissolution in biological fate and effects of nanoscale particles.** *Toxicol Sci* 2006, **90**:23-32.

32. Nel A, Xia T, Madler L, Li N: **Toxic potential of materials at the nanolevel.** *Science* 2006, **311**:622-627.
33. Rahman IA, Vejayakumaran P, Sipaut SC, Ismail J, Chee KC: **Size-dependent physicochemical and optical properties of silica nanoparticles.** *Materials Chemistry and Physics* 2009, **114**:328-332.
34. Xia T, Kovochich M, Brant J, Hotze M, Sempf J, Oberley T, Sioutas C, Yeh JI, Wiesner MR, Nel AE: **Comparison of the abilities of ambient and manufactured nanoparticles to induce cellular toxicity according to an oxidative stress paradigm.** *Nano Lett* 2006, **6**:1794-1807.
35. Eom HJ, Choi J: **Oxidative stress of silica nanoparticles in human bronchial epithelial cell, Beas-2B.** *Toxicol In Vitro* 2009, **23**:1326-1332.
36. Lin W, Huang YW, Zhou XD, Ma Y: **In vitro toxicity of silica nanoparticles in human lung cancer cells.** *Toxicol Appl Pharmacol* 2006, **217**:252-259.
37. Wang F, Gao F, Lan M, Yuan H, Huang Y, Liu J: **Oxidative stress contributes to silica nanoparticle-induced cytotoxicity in human embryonic kidney cells.** *Toxicol In Vitro* 2009, **23**:808-815.
38. Dostert C, Petrilli V, Van Bruggen R, Steele C, Mossman BT, Tschopp J: **Innate immune activation through Nalp3 inflammasome sensing of asbestos and silica.** *Science* 2008, **320**:674-677.
39. Hornung V, Bauernfeind F, Halle A, Samstad EO, Kono H, Rock KL, Fitzgerald KA, Latz E: **Silica crystals and aluminum salts activate the NALP3 inflammasome through phagosomal destabilization.** *Nat Immunol* 2008, **9**:847-856.
40. Ames BN: **Dietary carcinogens and anticarcinogens. Oxygen radicals and degenerative diseases.** *Science* 1983, **221**:1256-1264.
41. Harman D: **The aging process.** *Proc Natl Acad Sci USA* 1981, **78**:7124-7128.
42. Li Z, Hyseni X, Carter JD, Soukup JM, Dailey LA, Huang YC: **Pollutant particles enhanced H2O2 production from NAD(P)H oxidase and mitochondria in human pulmonary artery endothelial cells.** *Am J Physiol Cell Physiol* 2006, **291**:C357-365.
43. Wang T, Chiang ET, Moreno-Vinasco L, Lang GD, Pendyala S, Samet JM, Geyh AS, Breysse PN, Chillrud SN, Natarajan V, Garcia JG: **Particulate matter disrupts human lung endothelial barrier integrity via ROS- and p38 MAPK-dependent pathways.** *Am J Respir Cell Mol Biol* 2010, **42**:442-449.
44. Chamulitrat W, Stremmel W, Kawahara T, Rokutan K, Fujii H, Wingler K, Schmidt HH, Schmidt R: **A constitutive NADPH oxidase-like system containing gp91phox homologs in human keratinocytes.** *J Invest Dermatol* 2004, **122**:1000-1009.
45. Goldman R, Moshonov S, Zor U: **Generation of reactive oxygen species in a human keratinocyte cell line: role of calcium.** *Arch Biochem Biophys* 1998, **350**:10-18.
46. Goldman R, Moshonov S, Zor U: **Calcium-dependent PAF-stimulated generation of reactive oxygen species in a human keratinocyte cell line.** *Biochim Biophys Acta* 1999, **1438**:349-358.
47. Sekharam M, Cunnick JM, Wu J: **Involvement of lipoxygenase in lysophosphatidic acid-stimulated hydrogen peroxide release in human HaCaT keratinocytes.** *Biochem J* 2000, **346(Pt 3)**:751-758.
48. Sampath P, Pollard TD: **Effects of cytochalasin, phalloidin, and pH on the elongation of actin filaments.** *Biochemistry* 1991, **30**:1973-1980.
49. Lambeth JD: **NOX enzymes and the biology of reactive oxygen.** *Nat Rev Immunol* 2004, **4**:181-189.
50. Li Q, Zhang Y, Marden JJ, Banfi B, Engelhardt JF: **Endosomal NADPH oxidase regulates c-Src activation following hypoxia/reoxygenation injury.** *Biochem J* 2008, **411**:531-541.
51. Ushio-Fukai M: **Localizing NADPH oxidase-derived ROS.** *Sci STKE* 2006, **2006**:re8.
52. Morishige T, Yoshioka Y, Tanabe A, Yao X, Tsunoda S, Tsutsumi Y, Mukai Y, Okada N, Nakagawa S: **Titanium dioxide induces different levels of IL-1beta production dependent on its particle characteristics through caspase-1 activation mediated by reactive oxygen species and cathepsin B.** *Biochem Biophys Res Commun* 2010, **392**:160-165.
53. Fubini B, Hubbard A: **Reactive oxygen species (ROS) and reactive nitrogen species (RNS) generation by silica in inflammation and fibrosis.** *Free Radic Biol Med* 2003, **34**:1507-1516.
54. Meyer JW, Schmitt ME: **A central role for the endothelial NADPH oxidase in atherosclerosis.** *FEBS Lett* 2000, **472**:1-4.
55. Kawahara T, Kuwano Y, Teshima-Kondo S, Kawai T, Nikawa T, Kishi K, Rokutan K: **Toll-like receptor 4 regulates gastric pit cell responses to Helicobacter pylori infection.** *J Med Invest* 2001, **48**:190-197.
56. Schins RP: **Mechanisms of genotoxicity of particles and fibers.** *Inhal Toxicol* 2002, **14**:57-78.
57. Kagan VE, Tyurina YY, Tyurin VA, Konduru NV, Potapovich AI, Osipov AN, Kisin ER, Schwegler-Berry D, Mercer R, Castranova V, Shvedova AA: **Direct and indirect effects of single walled carbon nanotubes on RAW 264.7 macrophages: role of iron.** *Toxicol Lett* 2006, **165**:88-100.
58. Oberdorster G, Gelein R, Johnston C, Mercer P, Corson N, Finkelstein J: **Ambient ultra fine particles: Inducers of acute Lung injury? Relationships between respiratory disease and exposure to air pollution.** ILSI Press, Washington, DC; 1998, 216-229.
59. Terry LJ, Shows EB, Wente SR: **Crossing the nuclear envelope: hierarchical regulation of nucleocytoplasmic transport.** *Science* 2007, **318**:1412-1416.
60. Chen M, von Mikecz A: **Formation of nucleoplasmic protein aggregates impairs nuclear function in response to SiO2 nanoparticles.** *Exp Cell Res* 2005, **305**:51-62.
61. Lison D, Thomassen LC, Rabolli V, Gonzalez L, Napierska D, Seo JW, Kirsch-Volders M, Hoet P, Kirschhock CE, Martens JA: **Nominal and effective dosimetry of silica nanoparticles in cytotoxicity assays.** *Toxicol Sci* 2008, **104**:155-162.
62. Waters KM, Masiello LM, Zangar RC, Tarasevich BJ, Karin NJ, Quesenberry RD, Bandyopadhyay S, Teeguarden JG, Pounds JG, Thrall BD: **Macrophage responses to silica nanoparticles are highly conserved across particle sizes.** *Toxicol Sci* 2009, **107**:553-569.
63. Barnes CA, Elsaesser A, Arkusz J, Smok A, Palus J, Lesniak A, Salvati A, Hanrahan JP, Jong WH, Dziubaltowska E, *et al.*: **Reproducible comet assay of amorphous silica nanoparticles detects no genotoxicity.** *Nano Lett* 2008, **8**:3069-3074.
64. Inui S, Lee YF, Haake AR, Goldsmith LA, Chang C: **Induction of TR4 orphan receptor by retinoic acid in human HaCaT keratinocytes.** *J Invest Dermatol* 1999, **112**:426-431.

doi:10.1186/1743-8977-8-1
**Cite this article as:** Nabeshi *et al.*: Amorphous nanosilica induce endocytosis-dependent ROS generation and DNA damage in human keratinocytes. *Particle and Fibre Toxicology* 2011 **8**:1.